Inorg. Chem. **2008**, *47*, 5425−5440

Supramolecular Metal-Polypyridyl and Ru(II) Porphyrin Complexes: Photophysical, Electron Paramagnetic Resonance, and Electrochemical Studies

Fabrizia Fabrizi de Biani,*,† Emanuela Grigiotti,† Franco Laschi,† Piero Zanello,† Alberto Juris,‡ Luca Prodi,‡ Kelly S. Chichak,§ and Neil R. Branda§

Department of Chemistry, University of Siena, Siena, Via A. Moro, Siena 53100, Italy, Department of Chemistry, University of Bologna, Bologna, Via Selmi 2, Bologna 40126, Italy, and Department of Chemistry, Simon Fraser University, Burnaby, 8888 University Drive, Burnaby, B.C., V5A 1S6, Canada

Received September 18, 2007

A series of mixed-metal supramolecular porphyrin arrays in which the geometry of the central metal-polypyridyl moiety defines the spatial arrangement of two or more Ru(II)-porphyrin units through axial coordination have been prepared by employing self-assembly based protocols, and their photophysical and electrochemical properties have been studied. The electrochemical properties of the constituent parts of these arrays depend only on their own chemical environment, regardless of the nuclearity and the overall charge of the compound; in this way species with predetermined redox patterns can be obtained via the synthetic control of the self-assembly process. Interestingly, several of these arrays are luminescent both at room and at low temperatures, and in many cases core-to-periphery or periphery-to-core intramolecular energy transfer processes take place according to the nature of the central metal template.

Introduction

As evidenced by the efficiency that Nature's photosynthetic systems operate, the features that provide the most efficient means to harvest light and transform it into useable energy are structural sophistication and the inherent spatial control over these molecular components. It is well-known that the control over how these chromophoric building blocks are projected in space influences the resulting energy or electron transfer processes. For example, the bacterial photosynthetic reaction center consists of ten important components that are held and positioned noncovalently in the thylakoid membrane by three protein subunits.[1] The ten components responsible for efficient energy and electron transfer are two closely positioned bacteriochlorophyll-*a* molecules that make up the "special pair" electron donor, two monomeric bacteriochlorophyll-*a* molecules, two bacteriophrophytins, two ubiquinones, a carotenoid, and a nonheme iron component. Excitation of the special pair is achieved by rapid and efficient energy transfer from either the monomeric bacteriophrophytins and bacteriochlorophylls. After the light energy is transferred to the special pair, an electron is transferred to an electron acceptor which traps the excitation energy as a charge-separated species.[2] To afford efficient energy and electron transfer rates ($k \approx 3 \times 10^{11}$ s^{-1}) Nature positions the active porphyrinic species with a center-to-center separation of about 17 Å.[2d] The controlled center-to-center separation between chromophores maximizes the electronic interactions of the distance-dependent energy transfer processes. Apart from the obvious spatial control over these chromophores that mediates the process, the driving force for electron transfer processes relies on the relative differences in the redox potentials of all electron

* To whom correspondence should be addressed. E-mail: fabrizi@unisi.it. Fax: +39-0577-234233.
† University of Siena.
‡ University of Bologna.
§ Simon Fraser University.

(1) (a) Chang, C. H.; Elkabbani, O.; Tiede, D.; Norris, J.; Schiffer, M. *Biochemistry* **1991**, *30*, 5352. (b) Ermler, U.; Fritzsch, G.; Buchanan, S. K.; Michel, H. *Structure* **1994**, *2*, 925.

(2) (a) King, B. A.; McAnaney, T. B.; deWinter, A.; Boxer, S. G. *J. Phys. Chem. B* **2000**, *104*, 8895. (b) King, B. A.; de Winter, A.; McAnaney, T. B.; Boxer, S. G. *J. Phys. Chem. B* **2001**, *105*, 1856. (c) Jordanides, X. J.; Scholes, G. D.; Fleming, G. R. *J. Phys. Chem. B* **2001**, *105*, 1652. (d) Scholes, G. D.; Jordanides, X. J.; Fleming, G. R. *J. Phys. Chem. B* **2001**, *105*, 1640.

10.1021/ic7018428 CCC: $40.75
Published on Web 05/20/2008

donors and electron acceptors. To better understand the concerted energy and electron transfer processes that occur for these natural porphyrin-based systems, significant effort[3] has been put forth by the scientific community toward the study and design of small-molecular-based artificial photosynthetic models. The obvious challenge for their further development lies not only in the ability to prepare unique systems of photoelectro-active components but also in the ease by which their relative spatial arrangement is controlled. With this in mind, numerous polymolecular porphyrin-based assemblies, organized through the use of either covalent or noncovalent interactions, have been used to successfully model the sequence of events in photoinduced energy and electron transfer processes. For example, Sauvage[4] and coworkers have prepared and studied a complex library of artificial porphyrin systems constructed around a range of central transition metal complexes that display extraordinary function. These structurally confined systems are very modular with respect to the selection of the photoelectro-active components but are restricted by the manifold of covalent synthesis to afford only linearly arranged arrays. With this in mind, we became interested in exploring alternative coordinative methodologies to prepare similar porphyrin arrays with the added ability to control and rapidly change their spatial arrangements. More specifically, we have employed the virtues of self-assembly synthesis to rapidly construct linearly, tetrahedrally, and octahedrally arranged porphyrin arrays by using ambidentate ligands to template the position of divergent pyridyl Lewis bases that can confine metalloporphyrins around a central transition metal template through axial[5,6] coordination (Figure 1).

Our preliminary communications revealed[7] the ease by which linear and octahedral arrays can be prepared. In addition to these

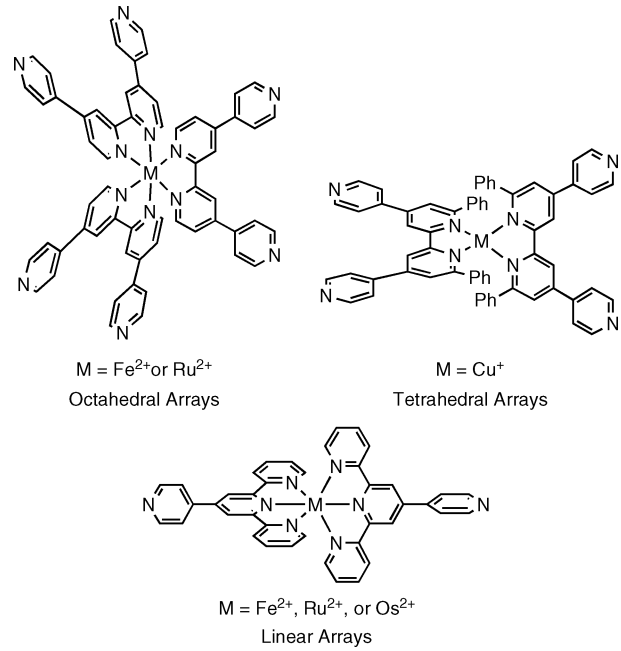

Figure 1. Central core transition metal templates used to prepare linear, tetrahedral, and octahedral porphyrin arrays.

porphyrin arrays, we also extended[8] this strategy to include the preparation of analogous assemblies based on axial coordination to ruthenium(II) carbonyl salophens. Herein, we describe the preparation of a tetrahedral Cu(I) porphyrin array and provide a complete comparison of the characteristic electrochemical and photophysical properties of this new tetrahedral array with those of the previously prepared linear and octahedral arrays built around Fe(II), Ru(II), and Os(II). Ruthenium- and osmium-based polypyridine and porphyrin complexes feature a rich electrochemical behavior together with very interesting photophysical properties.[9–11] In these compounds it is customary to use the localized MO (molecular orbital) approximation, so that oxidation and reduction are viewed as metal or ligand centered processes.[12] In mononuclear complexes of these families, oxidations are localized either on the metal center or on the porphyrin ring, while reductions take place either on the porphyrin ring or on the polypyridine ligands. In the case of polynuclear complexes, the study of the electrochemical properties can give a fingerprint of the supramolecular assembly, as a consequence of the fact that usually the redox processes featured by the single components are maintained in the final

(3) (a) Gust, D.; Moore, T. A.; Moore, A. L. *Acc. Chem. Res.* **1993**, *26*, 198. (b) Hunter, C. A.; Shannon, R. J. *Chem. Commun.* **1996**, 1361. (c) Drain, C. M.; Russell, K. C.; Lehn, J.-M. *Chem. Commun.* **1996**, 337. (d) Kumar, R. K.; Balasubramanian, S.; Goldberg, I. *Chem, Commun.* **1998**, 1435. (e) Wagner, R. W.; Seth, J.; Yang, S. I.; Kim, D.; Bocian, D. F.; Holten, D.; Lindsey, J. S. *J. Org. Chem.* **1998**, *63*, 5042. (f) Flamigni, L.; Barigelletti, F.; Armaroli, N.; Collin, J.-P.; Sauvage, J.-P.; Williams, J. A. G. *Chem.—Eur. J.* **1998**, *4*, 1744. (g) Mak, C. C.; Bampos, N.; Sanders, J. K. M. *Angew. Chem., Int. Ed.* **1998**, *37*, 3020. (h) Osuka, A.; Ikeda, M.; Shiratori, H.; Nishimura, Y.; Yamazaki, I. *J. Chem. Soc., Perkin Trans. II* **1999**, 1019. (i) Lammi, R. K.; Ambroise, A.; Balasubramanian, T.; Wagner, R. W.; Bocian, D. F.; Holten, D.; Lindsey, J. S. *J. Am. Chem. Soc.* **2000**, *122*, 7579. (j) Choi, M.-S.; Aida, T.; Yamazaki, T.; Yamazaki, I. *Angew. Chem., Int. Ed.* **2001**, *40*, 3194. (k) Gust, D.; Moore, T. A.; Moore, A. L. *Acc. Chem. Res.* **2001**, *34*, 40. (l) Song, H.; Kirmaier, C.; Schwartz, J. K.; Hindin, E.; Yu, L.; Bocain, D. F.; Lindsey, J. S.; Holten, D. *J. Phys. Chem. B* **2006**, *110*, 19121. (m) Yang, J.; Park, M.; Yoon, Z. S.; Hori, T.; Peng, X.; Aratani, N.; Dedecker, P.; Hotta, J.-I.; Uji-i, H.; Sliwa, M.; Hofkens, J.; Osuka, A.; Kim, D. *J. Am. Chem. Soc.* **2008**, *130*, 1879.

(4) (a) Harriman, A.; Sauvage, J.-P. *Chem. Soc. Rev.* **1996**, *25*, 41. (b) Baranoff, E.; Collin, J.-P.; Gruber, N.; Sauvage, J.-P. *Chem. Soc. Rev.* **2004**, *33*, 147.

(5) (a) For examples of other porphyrin arrays assembled through axial coordination, see Gardner, M.; Guerin, A. J.; Hunter, C. A.; Michelsen, U.; Rotger, C. *New J. Chem.* **1999**, 309. (b) Darling, S. L.; Mak, C. C.; Bampos, N.; Feeder, N.; Teat, S. J.; Sanders, J. K. M. *New J. Chem.* **1999**, *23*, 359. (c) Imamura, T.; Fukushima, K. *Coord. Chem. Rev.* **2000**, *198*, 133. (d) Michelsen, U.; Hunter, C. A. *Angew. Chem., Int. Ed.* **2000**, *39*, 764. (e) Redman, J. E.; Feeder, N.; Teat, S. J.; Sanders, J. K. M. *Inorg. Chem.* **2001**, *40*, 3217.

(6) (a) For representative examples of ruthenium(II) porphyrin arrays assembled through axial coordination, see Ikonen, M.; Guez, D.; Marvaud, V.; Markovitsi, D. *Chem. Phys. Lett.* **1994**, *231*, 93. (b) Funatsu, K.; Imamura, T.; Ichimura, A.; Sasaki, Y. *Inorg. Chem.* **1998**, *37*, 4986. (c) Prodi, A.; Indelli, M. T.; Kleverlaan, C. J.; Scandola, F.; Alessio, E.; Gianferrara, T.; Marzilli, L. G. *Chem.—Eur. J.* **1999**, *5*, 2668. (d) Prodi, A.; Chiorboli, C.; Scandola, F.; Iengo, E.; Alessio, E.; Dobrawa, R.; Würthner, F. *J. Am. Chem. Soc.* **2005**, *127*, 1454.

(7) (a) Chichak, K.; Branda, N. R. *Chem. Commun.* **1999**, 523. (b) Chichak, K.; Branda, N. R. *Chem. Commun.* **2000**, 1211.

(8) Chichak, K.; Jacquemard, U.; Branda, N. R. *Eur. J. Inorg. Chem.* **2002**, *2*, 357.

(9) Kadish, K. M. *Prog. Inorg. Chem.* **1986**, *34*, 435.

(10) Kalyanasundaram, K. *Photochemistry of Polypyridine and Porphyrin Complexes*; Academic Press: London, 1992.

(11) Juris, A.; Balzani, V.; Barigelletti, F.; Campagna, S.; Belser, P.; von Zelewsky, A. *Coord. Chem. Rev.* **1988**, *84*, 85.

(12) Balzani, V.; Juris, A.; Venturi, M.; Campagna, S.; Serroni, S. *Chem. Rev.* **1996**, *96*, 759.

Chart 1

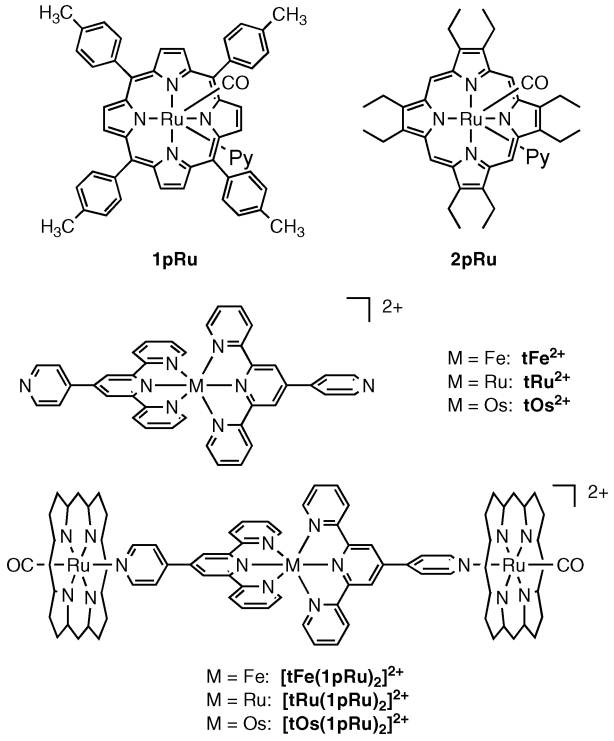

Chart 2

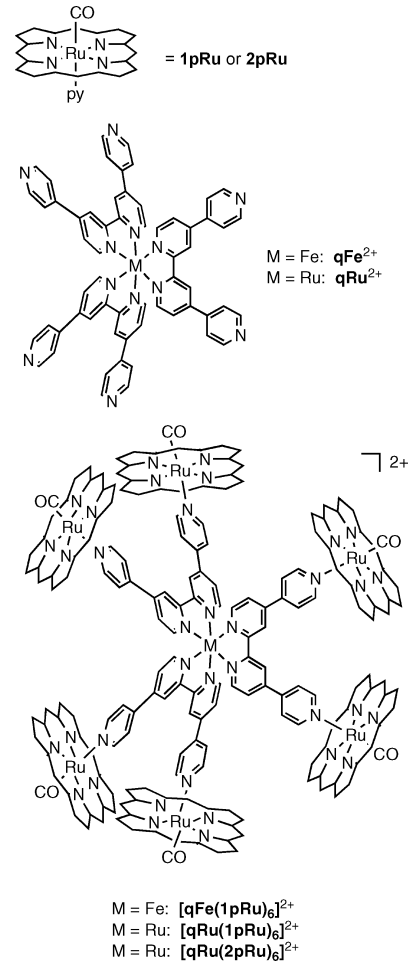

architecture, even if some small change in the electrode potential may occur. In practice, bridging ligands such as pytpy (pytpy = 4′-(4‴-pyridyl)-2,2′:6′,2″-terpyridine) and quad (quad = 4,4′-di(4″-pyridyl)-2,2′-bipyridine) do not allow substantial electronic communication between the connected units. Therefore, these ligands maintain their intrinsic redox properties in a supramolecular architecture, while allowing photoinduced energy- and electron-transfer processes to occur. The examined compounds are Ru(ttp)CO(py) (**1pRu**) (ttp = tetra-*p*-tolylporphyrin), Ru(oep)CO(py) (**2pRu**) (oep = octaethylporphyrin), $[Fe(pytpy)_2]^{2+}$ (**tFe²⁺**), $[Ru(pytpy)_2]^{2+}$ (**tRu²⁺**), $[Os(pytpy)_2]^{2+}$ (**tOs²⁺**), $[Fe(pytpy)_2(Ru(ttp)CO)_2]^{2+}$ (**[tFe(1pRu)₂]²⁺**), $[Ru(pytpy)_2(Ru(ttp)CO)_2]^{2+}$ (**[tRu(1pRu)₂]²⁺**), $[Os(pytpy)_2(Ru(ttp)CO)_2]^{2+}$ (**[tOs(1pRu)₂]²⁺**), $[Ru(quad)_3]^{2+}$ (**qRu²⁺**), $[Fe(quad)_3(Ru(ttp)CO)_6]^{2+}$ (**[qFe(1pRu)₆]²⁺**), $[Ru(quad)_3(Ru(ttp)CO)_6]^{2+}$ (**[qRu(1pRu)₆]²⁺**), $[Ru(quad)_3(Ru(oep)CO)_6]^{2+}$ (**[qRu(2pRu)₆]²⁺**), $[Cu(ph_4bipy)_2]^{+}$ (**1bCu⁺**) (ph_4bpy = 4,4′−6,6′-tertraphenyl-2,2′-bipyridine), $[Cu(ph_2quad)_2(Ru(ttp)CO)_4]^{+}$ (**[2bCu(1pRu)₄]⁺**) (ph_2quad = 4,4′:6,6′-(4″,4‴-dipyridyl)-(diphenyl)-2,2′-bipyridine). As shown in Charts 1–3the polynuclear species contain Ru(ttp)CO or Ru(oep)CO units axially linked to a central Fe(II), Ru(II), Os(II), or Cu(I) core complex using the bridging ligands pytpy, quad or ph_2quad.

Experimental Section

Synthesis. All solvents (Caledon) were distilled prior to use. All reagents and starting materials were purchased from Aldrich. 4′-(4‴-pyridyl)-2,2′:6′,2″-terpyridine (pytpy),[13,14] 5,10,15,20-tetratolylporphyrin,[15] Ru(ttp)(CO)(EtOH) (ttp = 5,10,15,20-tetratolylporphyrinato dianion),[16] Ru(ttp)(CO)(py) (**1pRu**),[7a] $[Fe(pytpy)_2][BF_4]_2$ (**tFe²⁺**),[14] $[Ru(pytpy)_2][PF_6]_2$ (**tRu²⁺**),[17] and $[Os(pytpy)_2][PF_6]_2$ (**tOs²⁺**)[17] (pytpy = 4′-(4‴-pyridyl)-2,2′:6′,2″-terpyridine), 1-cyanomethylpyridinium iodide,[18] 2-amino-6-phenyl-4,4′-bipyridine (**2**),[19] 4,4′:6,6′-(4″,4‴-dipyridyl)-(diphenyl)-2,2′-bipyridine (**2b**, ph_2quad), 4,4′:6,6′-tetraphenyl-2,2′-bipyridine (**1b**, ph_4bpy),[19] 4,4′-di(4″-pyridyl)-2,2′-bipyridine (**q**, quad),[20] $[Ru(quad)_3][PF_6]_2$ (**qRu²⁺**),[18] $[Fe(quad)_3][BF_4]_2$ (**qFe²⁺**),[20] 2,3,7,8,12,13,17,18-octaethylporphyrin,[21] Ru(oep)(CO)(EtOH) (oep = 2,3,7,8,12,13,17,18-octaethylporphyrinato dianion),[22] Ru(oep)(CO)(py) (**2pRu**),[23] and

(13) Constable, E. C.; Lewis, J.; Liptrot, M. C.; Raithby, P. R. *Inorg. Chim. Acta* **1990**, *178*, 47.
(14) Constable, E. C.; Thompson, A. M. W. C. *J. Chem. Soc., Dalton Trans.* **1992**, 2947.
(15) Alder, A. D.; Longo, F. R.; Finarelli, J. D.; Goldmacher, J.; Assour, J.; Koraskoff, L. *J. Org. Chem.* **1967**, *32*, 476.
(16) (a) Eaton, S. S.; Eaton, G. R. *Inorg. Chem.* **1977**, *16*, 72. (b) Rillema, D. P.; Nagle, J. K.; Barringer, L. F., Jr.; Meyer, T. J. *J. Am. Chem. Soc.* **1981**, *103*, 56.
(17) (a) Constable, E. C.; Thompson, A. M. W. C. *J. Chem. Soc., Dalton Trans.* **1994**, 1409. (b) Constable, E. C.; Thompson, A. M. W. C.; Tocher, D. A.; Daniels, M. A. M. *New. J. Chem.* **1992**, *16*, 855. (c) Maestri, M.; Armaroli, N.; Balzani, V.; Constable, E. C.; Thompson, A. M. W. C. *Inorg. Chem.* **1995**, *34*, 2759.
(18) Dürr, H.; Thiery, U.; Infelta, P. P.; Braun, A. M. *New J. Chem.* **1989**, *13*, 575.
(19) Kröhnke, F. *Synthesis* **1976**, 1.
(20) Morgan, R. J.; Baker, A. D. *J. Org. Chem.* **1990**, *55*, 1986.
(21) Paine, J. B., III; Kirshner, W. B.; Moskowitz, D. W.; Dolphin, D. *J. Org. Chem.* **1976**, *41*, 3857.
(22) Barley, M.; Becker, J. Y.; Domazetis, G.; Dolphin, D.; James, B. R. *Can. J. Chem.* **1983**, *61*, 2389.
(23) Barley, M.; Dolphin, D.; James, B. R.; Kirmaier, C.; Holten, D. *J. Am. Chem. Soc.* **1984**, *106*, 3937.

Chart 3

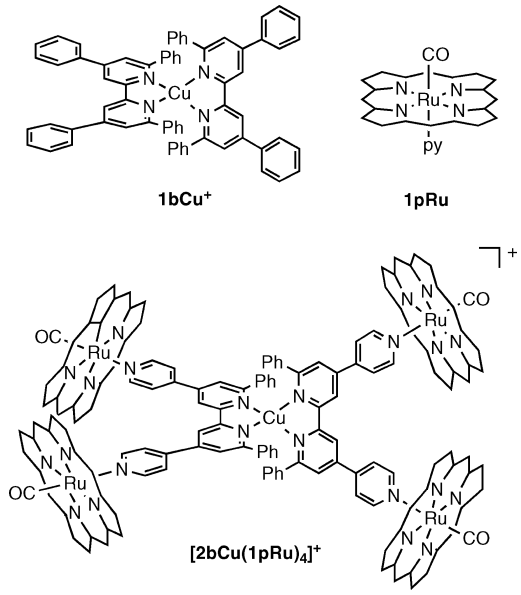

$[Ru(DMSO)_4Cl_2]$[24] were prepared as described in the literature (synthesis procedure and characterization of these compounds is reported in the Supporting Information). Solvents for NMR spectroscopic analysis (Cambridge Isotope Laboratories) were used as received. ^{1}H NMR spectroscopic characterizations were performed on a Varian Inova-500 instrument, working at 499.92, on a Varian Inova-400 instrument, working at 399.96, or on a Varian Inova-300 instrument, working at 299.96 MHz. Chemical shifts (δ) are reported in parts per million relative to tetramethylsilane using the residual solvent peak as a reference standard. FT-IR measurements were performed using a Nicolet Magna-IR 750 on solid samples using a microscope unless otherwise stated. Electrospray ionization mass spectra were recorded on a Micromass ZabSpec Hybrid Sector-TOF with positive mode electrospray ionization. The liquid carrier was infused into the electrospray source by means of a Harvard syringe pump at a flow rate of 10 μL/minute. The sample solution, in the same solvent, was introduced via a 1 μL-loop-injector. Prepurified nitrogen gas was used as a pneumatic aid and filtered air as the bath gas, heated at about 80 °C. For low resolution, the mass spectra were acquired by magnet scan at a rate of 5 s/decade at about 1000 resolution. For exact mass measurements, the spectra were obtained by a voltage scan over a narrow mass range at about 10000 resolution. Data acquisition and processing was achieved by using the OPUS software package on a Digital Alpha station with VMS operating system.

$[Fe(pytpy)_2(Ru(ttp)(CO))_2][BF_4]_2$ ($[tFe(1pRu)_2]^{2+}$). A solution of pytpy (13.0 mg, 4.19×10^{-2} mmol) in acetone (5.0 mL) was treated with 1.1 mol equiv of Ru(ttp)(CO)(EtOH) (40 mg, 4.74×10^{-2} mmol) followed by $Fe(BF_4)_2 \cdot 6H_2O$ (7.0 mg, 2.08×10^{-2} mmol) and stirred at ambient temperature for 22 h. The solvents were evaporated to dryness, and the resulting solid was dissolved in CH_2Cl_2. The product was precipitated by adding a mixture of Et_2O/pentane (20:80) and collected by filtration. The product was washed with a mixture of Et_2O/pentane (20:80) and dried under vacuum. Yield: 50.0 mg (98%). Mp > 300 °C (decomp); ^{1}H NMR (500 MHz, [D$_6$]acetone/CH_2Cl_2, 22 °C): δ = 8.66 (s, 16 H), 8.26 (s, 4 H), 8.19 (d, J = 7.0 Hz, 4 H), 8.08 (d, J = 7.0 Hz, 8 H), 7.96 (d, J = 7.0 Hz, 8 H), 7.53 (m, 12 H), 7.48 (d, J = 7.0 Hz, 8 H), 6.72 (m, J = 5.1 Hz, 4 H), 6.59 (m, 4 H), 6.11 (d, J = 5.5 Hz, 4 H), 2.63 (s, 24 H), 1.77 (d, J = 4.5 Hz, 4 H); ^{13}C NMR (125.7 MHz, [D$_6$]acetone/CH_2Cl_2, 22 °C) (21 of 22 signals): δ = 181.1, 160.6, 157.7, 152.9, 145.7, 145.5, 144.3, 140.0, 139.1, 137.6, 134.6, 134.4, 132.3, 127.9, 127.8, 127.6, 124.5, 122.2, 121.1, 120.4, 21.4; MS (ESI+): m/z = 1136 [2%, M − $2BF_4$]$^{2+}$, 737 [4%, M − TTP, $2BF_4$]$^{2+}$; Selected IR (microscope): ν = 1961 (CO) cm^{-1}.

$[Ru(pytpy)_2(Ru(ttp)(CO))_2][BF_4]_2$ ($[tRu(1pRu)_2]^{2+}$). A solution of **tRu**$[PF_6]_2$ (17.0 mg, 1.68×10^{-2} mmol) in acetone (5.0 mL) was treated with 2.5 mol equiv of Ru(ttp)(CO)(EtOH) (35 mg, 4.20×10^{-2} mmol) and stirred at ambient temperature for 22 h. The solvents were evaporated to dryness, and the resulting solid was dissolved in CH_2Cl_2. The product was precipitated by adding a mixture of Et_2O/pentane (20:80) and collected by filtration. The product was washed with a mixture of Et_2O/pentane (20:80) and dried under vacuum. Yield: 43.0 mg (98%). Mp > 300 °C (decomp); ^{1}H NMR (500 MHz, [D$_6$]acetone/CH_2Cl_2, 22 °C): δ = 8.66 (s, 16 H), 8.27 (d, J = 8.1 Hz, 4 H), 8.16 (s, 4 H), 8.08 (dd, J = 2.1, 7.8 Hz, 8 H), 7.93 (dd, J = 1.8, 7.8 Hz, 8 H), 7.62 (ddd, J = 1.5, 1.5, 7.8, 4 H), 7.55 (d, J = 8.5 Hz, 8 H) 7.47 (d, J = 8.1 Hz, 8 H), 6.91 (d, J = 5.1 Hz, 4 H), 6.85 (dd, J = 1.5, 5.7 Hz, 4 H), 6.00 (d, J = 7.5 Hz, 4 H), 2.64 (s, 24 H), 1.72 (d, J = 7.0 Hz, 4 H); ^{1}H NMR (300 MHz, [D$_6$]acetone, 22 °C): δ = 8.70 (s, 16 H), 8.44 (d, J = 8.1 Hz, 4 H), 8.40 (s, 4 H), 8.14 (dd, J = 2.1, 7.8 Hz, 8 H), 7.96 (dd, J = 1.8, 7.8 Hz, 8 H), 7.74 (dd, J = 1.5, 7.8 Hz, 4 H), 7.63 (d, J = 8.5 Hz, 8 H) 7.55 (d, J = 8.1 Hz, 8 H), 7.16 (d, J = 5.1 Hz, 4 H), 6.94 (dd, J = 1.5, 5.7 Hz, 4 H), 6.20 (dd, J = 1.8, 4.8 Hz, 4 H), 2.64 (s, 24 H), 1.79 (dd, J = 1.8, 4.8 Hz, 4 H); ^{13}C NMR (125.7 MHz, [D$_6$]acetone/CH_2Cl_2, 22 °C) (19 of 22 signals): δ = 157.5, 155.4, 153.1, 145.2, 144.1, 139.8, 138.3, 137.4, 134.4, 134.2, 132.1, 128.0, 127.7, 127.3, 124.9, 122.0, 121.1, 120.1, 21.3; MS (ESI+): m/z = 1664 [5%, M − TTP, PF_6]$^{1+}$, 1159 [12%, M − $2PF_6$]$^{2+}$, 867 [100%, M − 2TTP, PF_6]$^+$, 760 [15%, M − TTP, $2PF_6$]$^{2+}$; Selected IR (microscope): ν = 1959 (CO) cm^{-1}.

$[Os(pytpy)_2(Ru(ttp)(CO))_2][BF_4]_2$ ($[tOs(1pRu)_2]^{2+}$). A solution of **tOs**$[PF_6]_2$ (11.0 mg, 1.00×10^{-2} mmol) in acetone (5.0 mL) was treated with 3.0 mol equiv of Ru(ttp)(CO)(EtOH) (25 mg, 3.00×10^{-2} mmol) and stirred at ambient temperature for 22 h. The solvents were evaporated to dryness, and the resulting solid was dissolved in CH_2Cl_2. The product was precipitated by adding a mixture of Et_2O/pentane (20:80) and collected by filtration. The product was washed with a mixture of Et_2O/pentane (20:80) and dried under vacuum. Yield: 9.0 mg (98%). Mp > 300 °C (decomp); ^{1}H NMR (500 MHz, [D$_6$]acetone/CH_2Cl_2, 22 °C): δ = 8.66 (s, 16 H), 8.33 (d, J = 8.1 Hz, 4 H), 8.26 (s, 4 H), 8.08 (dd, J = 2.1, 7.8 Hz, 8 H), 7.93 (dd, J = 1.8, 7.8 Hz, 8 H), 7.57 (d, J = 8.5 Hz, 8 H), 7.52 (ddd, J = 1.5, 1.5, 7.8 Hz, 4 H), 7.48 (d, J = 8.1 Hz, 8 H), 6.87 (d, J = 5.1 Hz, 4 H), 6.81 (dd, J = 1.5, 5.7 Hz, 4 H), 6.03 (d, J = 1.5, 4.8 Hz, 4 H), 2.64 (s, 24 H), 1.72 (dd, J = 1.5, 4.8 Hz, 4 H); ^{1}H NMR (300 MHz, [D$_6$]acetone, 22 °C): δ = 8.70 (s, 16 H), 8.44 (d, J = 8.1 Hz, 4 H), 8.40 (s, 4 H), 8.14 (dd, J = 2.1, 7.8 Hz, 8 H), 7.96 (dd, J = 1.8, 7.8 Hz, 8 H), 7.74 (dd, J = 1.5, 7.8 Hz, 4 H), 7.63 (d, J = 8.5 Hz, 8 H) 7.55 (d, J = 8.1 Hz, 8 H), 7.16 (d, J = 5.1 Hz, 4 H), 6.94 (dd, J = 1.5, 5.7 Hz, 4 H), 6.20 (dd, J = 1.8, 4.8 Hz, 4 H), 2.64 (s, 24 H), 1.79 (dd, J = 1.8, 4.8 Hz, 4 H); ^{13}C NMR (125.7 MHz, [D$_6$]acetone/CH_2Cl_2, 22 °C) (19 of 22 signals): δ = 159.5, 154.9, 152.2, 145.1, 144.3, 140.0, 138.4, 137.6, 134.6, 134.3, 132.3, 128.2, 127.9, 127.5, 125.2, 122.2, 120.5, 120.2, 21.4; MS (ESI+): m/z = 1203 [25%, M − $2PF_6$]$^{2+}$, 957 [5%, M − 2TTP, PF_6]$^+$, 805 [45%, M − TTP, $2PF_6$]$^{2+}$, 406 [100%, M − 2TTP, $2PF_6$]$^{2+}$; Selected IR (microscope): ν = 1961 (CO) cm^{-1}.

$[Cu(ph_4bpy)_2][PF_6]$ (1bCu$^+$). To a stirred solution of **1b** (27.0 mg, 0.0590 mmol) in CH_3CN:MeOH (1:1, 5 mL) was added

(24) Evans, I. P.; Spencer, A.; Wilkinson, G. *J. Chem. Soc., Dalton Trans.* **1973**, 204.

$Cu(CH_3CN)_4PF_6$ (11.0 mg, 0.0295 mmol) which was accompanied with an immediate change in color of the solution from colorless to brown-red. The solution was concentrated to 2 mL, and ether was added to precipitate out the copper complex. The product was collected by vacuum filtration, washed with MeOH/Et_2O (1:1), and then dried under vacuum. Yield: 28.0 mg (83%). ^{1}H NMR (300 MHz, CD_3NO_2, 22 °C): δ = 8.16 (d, J = 1.5 Hz, 4 H), 7.79 (m, 12 H), 7.68 (m, 20 H), 7.08 (m, 4 H), 6.79 (t, J = 7.8 Hz, 8 H).

$[Cu(ph_2quad)_2(Ru(ttp)(CO))_4][PF_6]$ ($[2bCu(1pRu)_4]^+$). A solution of **2b** (10.0 mg, 2.17 × 10^{-2} mmol) in 5% acetone/CH_2Cl_2 (5.0 mL) was treated with 2.2 mol equiv of Ru(ttp)(CO)(EtOH) (37.0 mg, 4.35 × 10^{-2} mmol) followed by $Cu(CH_3CN)_4PF_6$ (4.0 mg, 1.07 × 10^{-2} mmol) and stirred at ambient temperature for 22 h. The solvents were evaporated to dryness, and the resulting solid was dissolved in CH_2Cl_2. The product was precipitated by adding a mixture of Et_2O/pentane (20:80) and collected by filtration. The product was washed with a mixture of Et_2O/pentane (20:80) and dried under vacuum. Yield: 45 mg (97%). Mp > 300 °C (decomp); ^{1}H NMR (500 MHz, [D_6]acetone/CD_2Cl_2, 22 °C): δ = 8.66 (s, 32 H), 8.11 (dd, J = 1.5, 7.5 Hz, 16 H), 7.84 (dd, J = 1.5, 7.5 Hz, 16 H), 7.63 (d, J = 7.5 Hz, 16 H), 7.45 (d, J = 7.5 Hz, 16 H), 6.88 (s, 4 H), 6.55 (d, J = 7.5 Hz, 8 H), 6.50 (s, 4 H), 6.06 (t, J = 7.5 Hz, 4 H), 5.87 (t, J = 7.5 Hz, 8 H), 5.45 (d, J = 7.0 Hz, 8 H), 2.67 (s, 48 H), 1.54 (d, J = 6.5 Hz, 8 H); ^{1}H NMR (300 MHz, CD_2Cl_2, 22 °C): δ = 8.67 (s, 32 H), 8.13 (dd, J = 1.5, 7.5 Hz, 16 H), 7.89 (dd, J = 1.5, 7.5 Hz, 16 H), 7.63 (d, J = 7.5 Hz, 16 H), 7.45 (d, J = 7.5 Hz, 16 H), 6.45 (d, J = 7.5 Hz, 8 H), 6.33 (s, 4 H), 6.28 (s, 4 H), 6.11 (t, J = 7.5 Hz, 4 H), 5.92 (t, J = 7.5 Hz, 8 H), 5.26 (d, J = 7.0 Hz, 8 H), 2.70 (s, 48 H), 1.60 (d, J = 6.5 Hz, 8 H); ^{13}C NMR (125.7 MHz, [D_6]acetone/CD_2Cl_2, 22 °C) (22 of 23 signals): δ = 156.6, 152.5, 145.0, 144.9, 143.9, 142.6, 139.7, 137.5, 137.1, 134.6, 133.9, 132.0, 131.7, 128.7, 127.8, 127.3, 126.9, 126.8, 122.2, 119.6, 118.4, 21.2; MS (ESI+): m/z = 4180 [1%, M − PF_6]$^+$, 3383 [1%, M − TTP, PF_6]$^+$, 2584 [4%, M − 2TTP, PF_6]$^+$, 1789 [5%, M − 3TTP, PF_6]$^+$, 987 [100%, M − 4TTP, PF_6]$^+$; Selected IR (microscope): ν = 1950 (CO) cm^{-1}.

$[Ru(quad)_3(Ru(ttp)(CO))_6][PF_6]_2$ ($[qRu(1pRu)_6]^{2+}$). A solution of **qRu**$[PF_6]_2$ (10.0 mg, 7.56 × 10^{-3} mmol) in acetone (5.0 mL) was treated with 6.3 mol equiv of Ru(ttp)(CO)(EtOH) (40.0 mg, 4.76 × 10^{-2} mmol) and stirred with gentle heating at 45 °C for 22 h. The solvents were evaporated to dryness, and the resulting solid was dissolved in CH_2Cl_2. The product was precipitated by adding a mixture of Et_2O/pentane (20:80) and collected by filtration. The product was washed with a mixture of Et_2O/pentane (20:80) and dried under vacuum. Yield: 43.0 mg (93%). Mp > 300 °C (decomp); ^{1}H NMR (300 MHz, [D_6]acetone, 22 °C): δ = 8.62 (s, 48 H), 8.13 (dd, J = 2.1, 7.8 Hz, 24 H), 7.75 (dd, J = 1.8, 7.8 Hz, 24 H), 7.71 (d, J = 8.5 Hz, 24 H), 7.45 (d, J = 8.1 Hz, 24 H), 7.27 (d, J = 1.8 Hz, 6 H), 6.53 (d, J = 6.3 Hz, 6 H), 6.02 (dd, J = 1.8, 6.0 Hz, 6 H), 5.16 (d, J = 6.9 Hz, 12 H), 2.73 (s, 72 H), 1.37 (d, J = 6.9 Hz, 12 H); ^{1}H NMR (300 MHz, CD_2Cl_2, 22 °C): δ = 8.59 (s, 48 H), 8.09 (dd, J = 2.1, 7.8 Hz, 24 H), 7.74 (dd, J = 1.8, 7.8 Hz, 24 H), 7.61 (d, J = 8.5 Hz, 24 H), 7.37 (d, J = 8.1 Hz, 24 H), 6.42 (d, J = 1.8 Hz, 6 H), 5.91 (d, J = 6.3 Hz, 6 H), 5.81 (dd, J = 1.8 Hz, 6.0 Hz, 6 H), 4.97 (dd, J = 1.5, 6.9 Hz, 12 H), 2.71 (s, 72 H), 1.35 (dd, J = 1.5, 6.9 Hz, 12 H); ^{13}C NMR (125.7 MHz, CD_2Cl_2, 22 °C): δ = 181.4, 156.8, 151.6, 145.2, 144.8, 144.5, 142.2, 140.3, 138.1, 134.9, 134.5, 132.2, 128.5, 128.0, 124.5, 122.5, 122.1, 120.1, 21.6; MS (ESI+): m/z = 2911 [10%, M − $2PF_6$]$^{2+}$, 2511 [13%, M − TTP, $2PF_6$]$^{2+}$, 2112 [12%, M − 2TTP, $2PF_6$]$^{2+}$, 1713 [10%, M − 3TTP, $2PF_6$]$^{2+}$, 1314 [12%, M − 4TTP, $2PF_6$]$^{2+}$, 915 [14%, M − 5TTP, $2PF_6$]$^{2+}$, 516 [100%, M − 6TTP, $2PF_6$]$^{2+}$; Selected IR (microscope): ν = 1968 (CO) cm^{-1}.

$[Ru(quad)_3(Ru(oep)(CO))_6][PF_6]_2$ ($[qRu(2pRu)_6]^{2+}$). A solution of **qRu**$[PF_6]_2$ (10.0 mg, 7.56 × 10^{-3} mmol) in acetone (5.0 mL) was treated with 6.3 mol equiv of Ru(oep)(CO)(EtOH) (35.0 mg, 4.76 × 10^{-2} mmol) and stirred at ambient temperature for 22 h. The solvents were evaporated to dryness, and the resulting solid was dissolved in CH_2Cl_2. The product was precipitated by adding a mixture of Et_2O/pentane (20:80) and collected by filtration. The product was washed with a mixture of Et_2O/pentane (20:80) and dried under vacuum. Yield: 40.0 mg (98%). Mp > 300 °C (decomp); ^{1}H NMR (300 MHz, [D_6]acetone, 22 °C): δ = 9.93 (s, 24 H), 6.94 (s, 6 H), 6.15 (d, J = 5.7 Hz, 6 H), 5.73 (d, J = 6.0 Hz, 6 H), 4.77 (d, J = 6.6 Hz, 12 H), 4.16 (m, 96 H), 1.93 (m, 144 H), 0.73 (d, J = 6.0 Hz, 12 H); ^{1}H NMR (300 MHz, CD_2Cl_2, 22 °C): δ = 9.93 (s, 24 H), 6.98 (s, 6 H), 6.53 (d, J = 5.7 Hz, 6 H), 5.76 (dd, J = 1.8, 6.3 Hz, 6 H), 4.81 (d, J = 6.9 Hz, 12 H), 4.16 (m, 96 H), 1.93 (m, 144 H), 0.73 (d, J = 6.0 Hz, 12 H); ^{13}C NMR (125.7 MHz, CD_2Cl_2, 22 °C): δ = 183.0, 156.5, 151.1, 145.1, 144.3, 142.9, 141.9, 141.4, 124.4, 121.3, 119.0, 98.9, 20.3, 19.0; MS (ESI+): m/z = 2503 [10%, M − $2PF_6$]$^{2+}$, 2171 [10%, M − OEP, $2PF_6$]$^{2+}$, 1839 [10%, M − 2OEP, $2PF_6$]$^{2+}$, 1509 [10%, M − 3OEP, $2PF_6$]$^{2+}$, 1178 [10%, M − 4OEP, $2PF_6$]$^{2+}$, 847 [15%, M − 5OEP, $2PF_6$]$^{2+}$, 516 [100%, M − 6OEP, $2PF_6$]$^{2+}$; Selected IR (microscope): ν = 1942 (CO) cm^{-1}.

$[Fe(quad)_3(Ru(ttp)(CO))_6][BF_4]_2$ ($[qFe(1pRu)_6]^{2+}$). A solution of **qFe**$[BF_4]_2$ (8.8 mg, 7.56 × 10^{-3} mmol) in acetone (5.0 mL) was treated with 6.3 mol equiv of Ru(ttp)(CO)(EtOH) (40.0 mg, 4.76 × 10^{-2} mmol) and stirred with gentle heating at 45 °C for 22 h. The solvents were evaporated to dryness, and the resulting solid was dissolved in CH_2Cl_2. The product was precipitated by adding a mixture of Et_2O/pentane (20:80) and collected by filtration. The product was washed with a mixture of Et_2O/pentane (20:80) and dried under vacuum. Yield: 38 mg (84%). Mp > 300 °C (decomp); ^{1}H NMR (300 MHz, [D_6]acetone/CD_2Cl_2, 22 °C): δ = 8.60 (s, 48 H), 8.08 (dd, J = 2.1, 7.8 Hz, 24 H), 7.72 (dd, J = 1.8, 7.8 Hz, 24 H), 7.62 (d, J = 8.5 Hz, 24 H), 7.40 (d, J = 8.1 Hz, 24 H), 7.13 (d, J = 1.8, 6 H), 5.98 (d, J = 6.3 Hz, 6 H), 5.89 (dd, J = 1.8, 6.0 Hz, 6 H), 5.08 (dd, J = 1.5, 6.9 Hz, 12 H), 2.71 (s, 72 H), 1.33 (dd, J = 1.5, 6.9 Hz, 12 H); ^{13}C NMR (125.7 MHz, [D_6]acetone/CD_2Cl_2, 22 °C): δ = 181.1, 160.6, 157.7, 152.9, 145.7, 145.4, 144.3, 142.9, 140.0, 139.1, 137.6, 134.6, 134.4, 132.3, 127.9, 127.8, 127.5, 124.4, 122.2, 121.1, 120.4, 21.4; ^{1}H NMR (300 MHz, CD_2Cl_2, 22 °C): δ = 8.59 (s, 48 H), 8.09 (dd, J = 2.1, 7.8 Hz, 24 H), 7.74 (dd, J = 1.8, 7.8 Hz, 24 H), 7.61 (d, J = 8.5 Hz, 24 H), 7.37 (d, J = 8.1 Hz, 24 H), 6.42 (d, J = 1.8 Hz, 6 H), 5.91 (d, J = 6.3 Hz, 6 H), 5.81 (dd, J = 1.8, 6.0 Hz, 6 H), 4.97 (dd, J = 1.5, 6.9 Hz, 12 H), 2.71 (s, 72 H), 1.35 (dd, J = 1.5, 6.9 Hz, 12 H); MS (ESI+): m/z = 2889 [10%, M − $2BF_4$]$^{2+}$, 2489 [15%, M − TTP, $2BF_4$]$^{2+}$, 2089 [20%, M − 2TTP, $2BF_4$]$^{2+}$, 1689 [20%, M − 3TTP, $2BF_4$]$^{2+}$, 1292 [20%, M − 4TTP, $2BF_4$]$^{2+}$, 892 [25%, M − 5TTP, $2BF_4$]$^{2+}$, 493 [100%, M − 6TTP, $2BF_4$]$^{2+}$; Selected IR (microscope): ν = 1953 (CO) cm^{-1}.

$[Fe(quad)_3(Ru(oep)(CO))_6][BF_4]_2$ ($[qFe(2pRu)_6]^{2+}$). A solution of **qFe**$[BF_4]_2$ (11.0 mg, 9.49 × 10^{-3} mmol) in acetone (5.0 mL) was treated with 6.3 mol equiv of Ru(oep)(CO)(EtOH) (42.0 mg, 5.98 × 10^{-2} mmol) and stirred with gentle heating at 45 °C for 22 h. The solvents were evaporated to dryness, and the resulting solid was dissolved in CH_2Cl_2. The product was precipitated by adding a mixture of Et_2O/pentane (20:80) and collected by filtration. The product was washed with a mixture of Et_2O/pentane (20:80) and dried under vacuum. Yield: 32 mg (70%). Mp > 300 °C (decomp); ^{1}H NMR (500 MHz, [D_6]acetone, 22 °C): δ = 9.96 (s, 24 H), 6.95 (s, 6 H), 5.83 (d, J = 6.5 Hz, 6 H), 5.72 (d, J = 6.0 Hz, 6 H), 4.81 (d, J = 6.5 Hz, 12 H), 4.10 (m, 96 H), 1.96 (m, 144

Table 1. Crystal Data and Summary of Intensity Data Collection and Structure Refinement for **1bCu**$^+$

formula	$C_{68.5}H_{49}ClCuF_6N_4P$
formula weight	1172.08
temperature (°C)	−80
radiation (λ [Å])	graphite-monochromated Mo Kα (0.71073)
crystal dimensions (mm)	0.42 × 0.21 × 0.04
crystal system	triclinic
space group	$P\bar{1}$ (No. 2)
unit cell parameters	
a (Å)	14.579 (2)
b (Å)	15.427 (2)
c (Å)	16.578 (3)
α (deg)	73.012 (3)
β (deg)	66.023 (3)
γ (deg)	65.533 (3)
V (Å^3)	3066.4 (8)
Z	2
ρ_{calcd} (g cm^{-3})	1.269
μ (mm^{-1})	0.487
θ range for data collected (deg)	1.23−26.50
data collection 2θ limit (deg)	53.00
scan type	ϕ rotations (0.3°)/ω scans (0.3°) (30 s exposures)
total data collected	15340 ($-10 \le h \le 18$, $-13 \le k \le 19$, $-20 \le l \le 20$)
independent reflections	12449 ($R_{int} = 0.0538$)
refinement method	full-matrix least-squares on F^2 (*SHELXL-97*)
data/restraints/parameters	12449 [$F_o^2 \ge -3\sigma(F_o^2)$]/5/767
goodness-of-fit (S)[a]	0.968 [$F_o^2 \ge -3\sigma(F_o^2)$]
final R indices[b]	
R_1 [$F_o^2 \ge 2\sigma(F_o^2)$]	0.1121
wR_2 [$F_o^2 \ge -3\sigma(F_o^2)$]	0.3456

[a] $S = [\Sigma w(F_o^2 - F_c^2)^2/(n-p)]^{1/2}$ (n = number of data; p = number of parameters varied; $w = [\sigma^2(F_o^2) + (0.1727P)^2]^{-1}$ where $P = [\mathrm{Max}(F_o^2, 0) + 2F_c^2]/3$). [b] $R_1 = \Sigma||F_o| - |F_c||/\Sigma|F_o|$; $wR_2 = [\Sigma w(F_o^2 - F_c^2)^2/\Sigma w(F_o^4)]^{1/2}$.

H), 0.69 (d, J = 7.0 Hz, 12 H); ^{1}H NMR (300 MHz, CD_2Cl_2, 22 °C): δ = 9.93 (s, 24 H), 6.98 (s, 6 H), 6.53 (d, J = 5.7 Hz, 6 H), 5.76 (dd, J = 1.8, 6.3 Hz, 6 H), 4.81 (d, J = 6.9 Hz, 12 H), 4.16 (m, 96 H), 1.93 (m, 144 H), 0.73 (d, J = 6.0 Hz, 12 H); ^{13}C NMR (125.7 MHz, [D$_6$]acetone, 22 °C): δ = 183.0, 158.5, 153.7, 145.1, 145.0, 142.9, 141.9, 141.4, 124.1, 120.8, 119.1, 98.9, 20.3, 19.0; MS (ESI+): m/z = 2479 [10%, M − 2BF$_4$]$^{2+}$, 2146 [5%, M − OEP, 2BF$_4$]$^{2+}$, 1815 [10%, M − 2OEP, 2BF$_4$]$^{2+}$, 1487 [5%, M − 3OEP, 2BF$_4$]$^{2+}$, 1156 [10%, M − 4OEP, 2BF$_4$]$^{2+}$, 825 [15%, M − 5OEP, 2BF$_4$]$^{2+}$, 493 [100%, M − 6OEP, 2BF$_4$]$^{2+}$; Selected IR (microscope): ν = 1941 (CO) cm^{-1}.

X-ray Crystallography. The crystallographic data for the complex **1bCu**$^+$ are shown in Table 1. Crystals of **1bCu**$^+$ were grown from a CH_2Cl_2 solution. X-ray diffraction data were collected on a Bruker PLATFORM/SMART 1000 CCD at 193 K using a graphite-monochromated Mo Kα radiation (λ = 0.71073 Å) by taking ω scans at 0.2° intervals. The cell parameters were obtained from the least-squares refinement of 4276 centered reflections using the SMART program. The structure was solved by direct methods/fragment search using the computer program DIRDIF96 and refined by full-matrix least-squares with anisotropic displacement parameters for the non-hydrogen atoms using the computer program SHELXL97.[25] Distances within the disordered solvent dichloromethane molecule were assigned fixed idealized values: d(Cl1S−C1S) = d(Cl2S−C1S) = d(Cl3S−C1S) = 1.80 Å; d(Cl1S···Cl2S) = d(Cl1S···Cl3S) = 2.95 Å (Cl1S and C1S were refined with an occupancy factor of 0.5; Cl2S and Cl3S are two sites for the disordered half-occupancy chlorine atom; thus, each were refined with an occupancy factor of 0.25). Hydrogen atoms were introduced in their idealized positions as indicated by the sp^2 geometries of their attached carbon atoms.

Electrochemistry. Anhydrous 99.9%, HPLC grade dichloromethane for electrochemistry was purchased from Aldrich. The supporting electrolyte was electrochemical grade [NBu$_4$][PF$_6$] obtained from Fluka. Cyclic voltammetry was performed in a three-electrode cell having a platinum working electrode surrounded by a platinum-spiral counter electrode and the aqueous saturated calomel reference electrode (SCE) mounted with a Luggin capillary. Either a BAS 100A or a BAS 100W electrochemical analyzer was used as a polarizing unit. Controlled potential coulometry was performed in an H-shaped cell with anodic and cathodic compartments separated by a sintered-glass disk. The working macroelectrode was platinum gauze; a mercury pool was used as the counter electrode. All reported potential values are referred to the saturated calomel electrode (SCE). Under the present experimental conditions, the one-electron oxidation of ferrocene occurs at $E^{\circ\prime} = +0.39$ V.

Spectroelectrochemistry. UV−vis spectroelectrochemical measurements were carried out using a Perkin-Elmer Lambda 900 UV−vis spectrophotometer and an optically transparent thin-layer electrode cell (OTTLE cell) equipped with a Pt-minigrid working electrode (32 wires/cm), Pt minigrid auxiliary electrode, Ag wire pseudoreference, and CaF_2 windows.[26] During the microelectrolysis procedures, the electrode potential was controlled by an Amel potentiostat 2059 equipped with an Amel function generator 568. Nitrogen-saturated CH_2Cl_2 solutions of the compound under study were used with [NBu$_4$][PF$_6$] (0.2 mol dm^{-3}) as supporting electrolyte.

EPR. X-band electron spin resonance (ESR) spectra were recorded with an ER 200 D-SRC Bruker spectrometer operating at ν = 9.62 GHz using a HS Brucker rectangular cavity. The control of the operational frequency was obtained with a Hewlett-Packard x 5−32 B wavemeter, and the magnetic field was calibrated with a DPPH (diphenyl-picryl-hydrazyl) free radical as a suitable field marker. The control of the temperature was obtained with a Bruker ER 4111 VT device (±1K). The g values are referred to DPPH (g = 2.0036) used as external standard reference.

Photophysical Studies. Photophysical experiments were conducted in deaerated CH_2Cl_2 solution at room temperature and in CH_2Cl_2/$CHCl_3$ 1:1 v/v matrix at 77 K. Uncorrected emission spectra, corrected excitation spectra, and phosphorescence lifetimes were obtained with a Perkin-Elmer LS50 spectrofluorimeter. Emission spectra at 77 K were recorded using quartz tubes immersed in a quartz Dewar flask filled with liquid nitrogen. Corrections for instrumental response, inner filter effects, and phototube sensitivity were performed as previously described.[27]

Results and Discussion

Synthesis. Our initial investigations concerning the formation of tetrahedral Cu(I) porphyrin arrays employed the same self-assembly strategy we used to prepare the linear and octahedral arrays based on suitable central metal templates and an appropriate divergent tetrapyridyl chelating ligand (Scheme 1).

During these investigations, we also explored the utility of the divergent ligand quad (**q**) in generating the central tetrahedral complex **qCu**$^+$ by reacting **q** with [Cu(CH$_3$-

(25) Sheldrick, G. M. *Acta Crystallogr.* **1990**, *A46*, 467.

(26) Krejčik, M.; Daněk, M.; Hartl, F. *J. Electroanal. Chem.* **1991**, *317*, 179.

(27) Juris, A.; Prodi, L. *New J. Chem.* **2001**, *25*, 1132.

Scheme 1

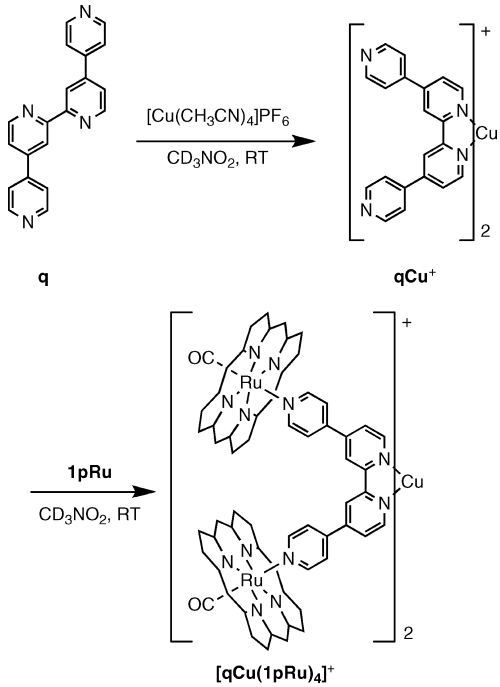

$CN)_4]PF_6$ in a 2:1 molar ratio in deuterated nitromethane at room temperature until the desired core complex was evident by ^{1}H NMR spectroscopy. Unfortunately, the generated spectra were complicated by extremely broad resonances, and, instead of isolating this tetrahedral core complex, this intermediate product was treated *in situ* with four equivalents of **1pRu** to produce the desired tetrahedral array $[\mathbf{qCu(1pRu)_4}]^+$ (Scheme 1). The diagnostic signals for axial coordination, upfield shifts of $\Delta\delta = -7.0$ and -2.0 ppm for the α and β protons of the axially bound pyridine, respectively, were observed as these protons lie directly over the porphyrin's anisotropic ring current, but, because of their extremely broad appearance, the complete characterization of this product was rather difficult. As such, complexes $\mathbf{qCu}^+$ and $[\mathbf{qCu(1pRu)_4}]^+$ could not be isolated even when rigorously anhydrous and anaerobic conditions were maintained, and these results suggested that the ligand **q** was improperly designed to bind Cu(I). All difficulties encountered in attempting to isolate the core fragment $\mathbf{qCu}^+$ and the tetrahedral array $[\mathbf{qCu(1pRu)_4}]^+$ can be attributed to improper metal/ligand pairing between Cu(I) and **q** which influences the complex's stability. This instability is due[28] to the absence of bulky noncoordinating groups adjacent to the diimine nitrogen atoms on the ligand that limit the access of Lewis bases from an axial approach which can result in a distortion of the initial tetrahedral geometry around the Cu(I) core. This distortion promotes the oxidation of the diamagnetic Cu(I) to paramagnetic Cu(II) species. In the presence of bulky noncoordinating groups in the 6,6′-positions on the bipyridine ligand, the axial site is blocked and the geometric distortion is prevented because the severe

(28) (a) Burke, P. J.; McMillin, D. R.; Robinson, W. R. *Inorg. Chem.* **1980**, *19*, 1211. (b) Pallenberg, A. J.; Koenig, K. S.; Barnhart, D. M. *Inorg. Chem.* **1995**, *34*, 2833. (c) Meyer, M.; Albrecht-Gary, A.-M.; Dietrich-Buchecker, C. O.; Sauvage, J.-P. *Inorg. Chem.* **1999**, *38*, 2279.

Scheme 2

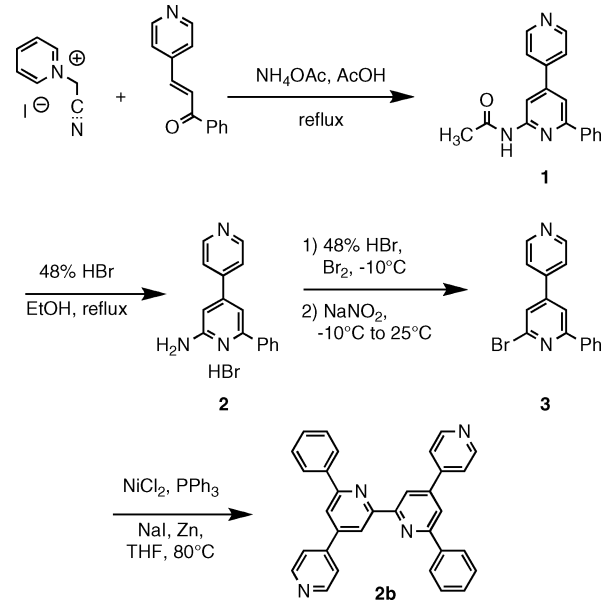

Scheme 3

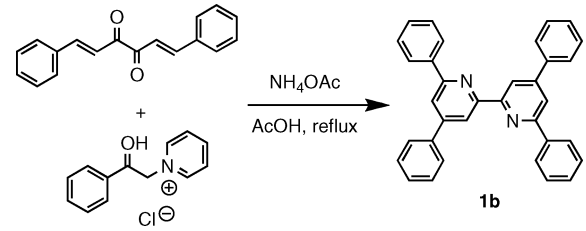

interligand repulsions that occur inhibit this process. To overcome the ligand/metal pair mismatch described for the core complex $\mathbf{qCu}^+$, the bis(phenyl)bipyridine ligand **2b** was synthesized (Scheme 2).

Cyclocondensation of the ketopyridine with 1-cyanomethylpyridinium iodide[18] using the protocol described by Kröhnke afforded gram quantities of the acetamidobipyridine **1**.[19] The acetamide was hydrolyzed with 48% hydrobromic acid into the known amine salt **2**,[19] which was cleanly converted to the bromide **3** using Sandmeyer conditions followed by nickel(II)-catalyzed coupling to yield the final tetrapyridine **2b**. The *in situ* generation of the tetrahedral core complex $\mathbf{2bCu}^+$ was monitored using ^{1}H NMR spectroscopy when ligand **2b** was reacted with $[Cu(CH_3CN)_4]PF_6$ in a 2:1 molar ratio in deuterated nitromethane. Surprisingly, instead of observing the clean conversion into the Cu(I) complex the spectrum was complicated by the appearance of broad signals. Also, the expected change in color from colorless to red-brown, which is evidence for proper Cu(I) chelation, did not occur. Instead, the reaction produced a light green solution containing a green precipitate. To determine the origin of these unexpected problems concerning the stability of the tetrahedral complex using this suitably substituted bipyridine, the known tetraphenylbipyridine **1b** analog was prepared (Scheme 3).[19]

When subjected to the same protocol as already described for the formation of the tetrahedral complex $\mathbf{2bCu}^+$, ligand **1b** readily reacted with $[Cu(CH_3CN)_4]PF_6$ producing a red-

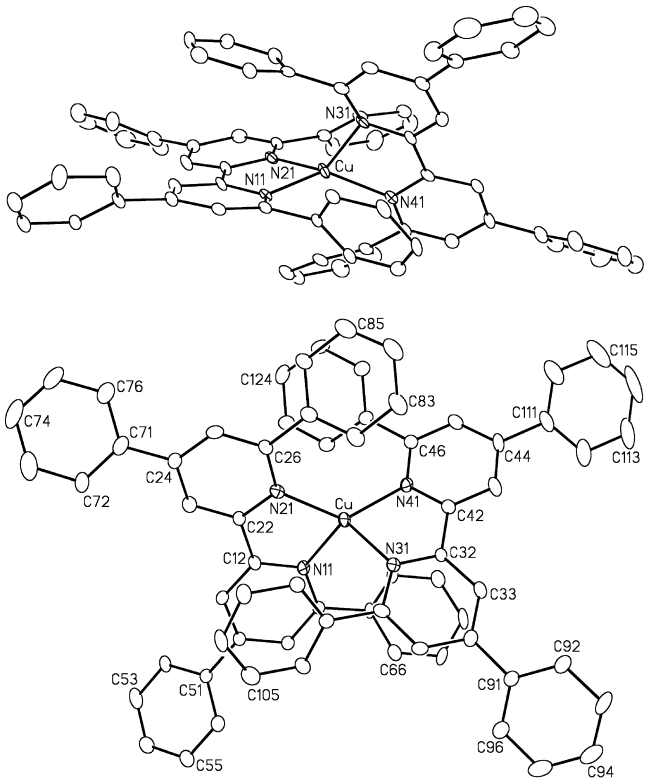

Figure 2. Perspective view (top) and top view (bottom) of the **1bCu**$^+$ ion showing the atom labelling scheme. Non-hydrogen atoms are represented by Gaussian ellipsoids at the 20% probability level. Hydrogen atoms are not shown.

Table 2. Selected Bond Distances (Å) and Angles (deg) for **1bCu**$^+$

atom1	atom2	distance	atom1	atom2	atom3	angle
Cu	N11	2.027(6)	N11	Cu	N21	83.1(2)
Cu	N21	2.008(7)	N11	Cu	N31	103.7(2)
Cu	N31	2.047(6)	N11	Cu	N41	131.8(2)
Cu	N41	2.005(6)	N21	Cu	N31	130.2(3)
			N21	Cu	N41	129.7(3)
			N31	Cu	N41	81.9(3)

brown solution which supports the formation of the tetrahedral Cu(I) complex [**1bCu**]PF_6. The higher stability of complex [**1bCu**]PF_6 provided single crystals suitable for X-ray analysis shown in Figure 2 (X-ray data and selected bond distances/angles are reported in Tables 1 and 2). The structure confirms the anticipated bis-ligand formulation of the Cu(I) complex. The structure also reveals that, in the solid state, the copper(I) complex adopts a distorted tetrahedral geometry (pseudotetrahedral). Each bipyridine ligand coordinates in a bidentate manner via the pyridines, but the dihedral angle between the planes defined by copper and each set of bipyridyl nitrogens is about 65°, so that the planes are far from being perpendicular. The distortion is partly due to how the bipyridine ligands impose small bite angles for the two N−Cu−N chelates of about 82°, which causes the other NCuN angles to vary between 103° and 132°. These angles force a geometry around Cu(I) that is appreciably distorted from regular tetrahedral, at least in the solid state, and the distortion allows potential access to the metal center by incoming ligands.

Having a better understanding of the coordination algorithm of ligand **2b**, we could form the final tetrahedral array

Scheme 4

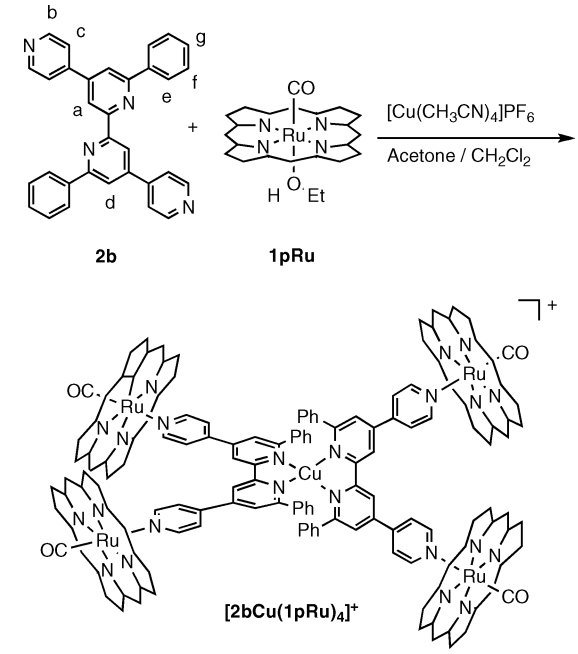

([**2bCu(1pRu)$_4$**]$^+$) and isolate it as a purple air-stable solid following a one-pot protocol. The previous observations suggested that the terminal pyridines of ligand **2b** were involved in the self-assembly coordination algorithm with copper(I), and, thus, preassembling the ruthenium porphyrin units onto the terminal pyridine nitrogens prior to assembling the final array should mitigate their involvement in the self-assembly process. Thus, treatment of **2b** with two molar equivalents of Ru(ttp)(CO)(EtOH) followed by 0.5 mol equiv of $[Cu(CH_3CN)_4]PF_6$ immediately resulted in the formation of ([**2bCu(1pRu)$_4$**]$^+$) in greater than 95% yield (Scheme 4 and Figure 3).

The copper(I) binding event results in the shifting of the resonances of the central core complex (protons H_a, H_d, H_e, H_f, and H_g in Scheme 4) into a visible region of the spectrum that are well separated from neighboring signals. Their final chemical shifts result from a combination of two effects: (1) the additive effect of the anisotropic ring currents of the four metalloporphyrins that point toward the core of the complex, and (2) the introduction of multiple face-to-face π-stacking effects between the flanking aromatic rings. The combination of these three effects results in shifting all of the signals for the core complex upfield from their original chemical shifts. The synthesis of the copper(I) tetrahedral array exemplifies the power of self-assembly synthesis to limit additional synthetic steps and rapidly form products in high yields. The tetrahedral array ([**2bCu(1pRu)$_4$**]$^+$) was also characterized by electrospray mass spectrometry (ESI-MS) using a CH_2Cl_2/nitromethane solvent mixture (Figure 4). The peak for the parent cation at $m/z = 4180$ $[M - PF_6]^+$ was seen along with peaks corresponding to consecutive loss of porphyrin units ($m/z = 3383$, 2584, and 1789). The isotopic abundance of each peak displayed the typical 1.0 peak separation of singly charged species.

Electrochemical Properties. Let us first consider the redox aptitude of the complexes illustrated in Chart 1. The

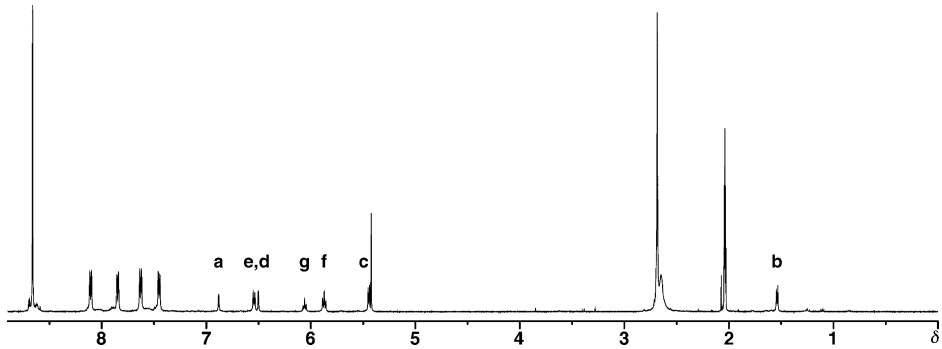

Figure 3. ^{1}H NMR (300 MHz, [D_6]acetone/CD_2Cl_2) spectra of **[2bCu(1pRu)$_4$]$^+$**. Peak assignments correspond to the atom labels in Scheme 4.

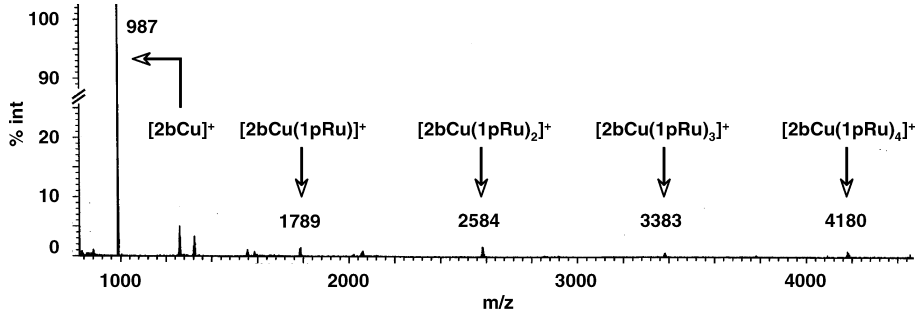

Figure 4. ESI mass spectrum of **[2bCu(1pRu)$_4$]$^+$** from CH_2Cl_2/CH_3NO_2.

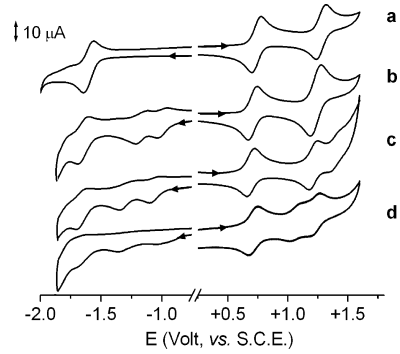

Figure 5. Cyclic voltammetric responses recorded at platinum electrode in CH_2Cl_2 solution containing: (a) **1pRu** (0.4×10^{-3} mol dm^{-3}), (b) **tFe(1pRu)$_2$]$^{2+}$** (0.4×10^{-3} mol dm^{-3}), (c) **[tRu(1pRu)$_2$]$^{2+}$** (0.6×10^{-3} mol dm^{-3}), (d) **[tOs(1pRu)$_2$]$^{2+}$** (0.5×10^{-3} mol dm^{-3}). [NBu_4][PF_6] (0.2 mol dm^{-3}) supporting electrolyte. Scan rate, 0.2 V s^{-1}.

cyclic voltammetric profile of the building block **1pRu** is shown in Figure 5a, which also displays the cyclic voltammetric responses of the trinuclear compounds **[tM(1pRu)$_2$]$^{2+}$** (M = Fe, Ru, Os).

The cyclic voltammogram (CV) of **1pRu** exhibits two subsequent oxidations both possessing features of chemical and electrochemical reversibility in the time-scale of cyclic voltammetry (i_{pc}/i_{pa} is constantly close to 1; $\Delta E_p = 80$ mV at 0.2 V s^{-1}). Controlled potential coulometry in correspondence to the first anodic process ($E_w = +1.0$ V) showed the consumption of one electron *per* molecule. Upon bulk oxidation, the ruby-red solution turns green, and the stable cation **[1pRu]$^+$** forms, as attested by the CVs which appear complementary to the original ones. In contrast, CVs recorded after the bulk electrolysis in correspondence to the second anodic process ($E_w = +1.4$ V) showed decomposition of the electrogenerated dication. Upon reduction, a single, partially chemically reversible, one electron process is detected. It is known that the oxidation of carbonyl ruthenium(II) porphyrins occurs at the ligand ring to give a π-cation radical species.[29] In the present case, EPR spectra recorded on the one-electron oxidized species support the claim that the first oxidation involves the removal of one electron from the π-system of the porphyrin core. The second oxidation possibly involves the removal of one electron from the ruthenium d-orbitals, as suggested by a comparison of the redox potential value with those reported for the family of related complex Ru(pX-TTP)(CO) (X = MeO, Me, F, Br, Cl).[29b] A very similar redox behavior has been observed for **2pRu**, which also undergoes two oxidations; in this case, however, the reduction process is cathodically shifted and is not observed in the experimental window.

As deducible from Table 3, which compiles the formal electrode potentials of the redox changes exhibited by complexes reported in Chart 1, complexes **tM^{2+}** (M = Fe, Ru, Os) undergo one metal-centered oxidation and two ligand-centered reductions, as it generally happens for metal-polypyridine complexes.[12]

The coulometrically measured removal of one electron from the complexes occurs at potentials matching the order Ru > Fe > Os,[12,30] as had been previously observed for similar compounds. The electron removal is accompanied by the adsorption of the oxidized species onto the electrode. As far as the two pytpy-centered one-electron reductions, the first one is almost unaffected by the nature of the metal,

(29) (a) Brown, G. M.; Hopf, F. R.; Ferguson, J. A.; Meyer, T. J.; Whitten, D. G. *J. Am. Chem. Soc.* **1973**, *95*, 5939. (b) Rillema, D. P.; Nagle, J. K.; Barringer, L. F.; Meyer, T. J. *J. Am. Chem. Soc.* **1981**, *103*, 56. (c) Morishima, I.; Takamuki, Y.; Shiro, Y. *J. Am. Chem. Soc.* **1984**, *106*, 7666.

(30) (a) Sun, S.-S.; Lees, A. J. *Inorg. Chem.* **2001**, *13*, 3154. (b) Winkler, K.; Płońska, M. E.; Rećko, K.; Dobrzyński, L. *Electrochim. Acta* **2006**, *51*, 4544.

Table 3. Formal Electrode Potentials (V vs SCE) for the Redox Processes Exhibited by CH_2Cl_2 Solutions of the Complexes Shown In Chart 1

compound	oxidation processes				reduction processes[a]		
1pRu		+1.28		+0.73			−1.62
2pRu			+1.18	+0.59			
tFe^{2+}		+1.22			−1.10	−1.26	
tRu^{2+}	+1.38				−1.14	−1.40	
tOs$^{2+>}$			+1.03		−1.10	−1.41	
[tFe(1pRu)$_2$]$^{2+}$		+1.23[b]		+0.71[c]	−1.00	−1.21	−1.65[c]
[tRu(1pRu)$_2$]$^{2+}$	+1.37	+1.21[c]		+0.69[c]	−1.07	−1.33	−1.68[c]
[tOs(1pRu)$_2$]$^{2+}$		+1.23[c]	+1.05	+0.72[c]	−1.02	−1.36	−1.69[c]

[a] Complicated by a subsequent chemical reaction. [b] Three-electron process. [c] Two-electron process.

Table 4. Formal Electrode Potentials (V vs SCE) for the Redox Processes Exhibited by CH_2Cl_2 Solutions of the Complexes Shown in Chart 2

compound	oxidation processes				reduction processes[a]		
qRu^{2+}	+1.4[a]				−1.12	−1.27	−1.51
[qFe(1pRu)$_6$]$^{2+}$		+1.25[b]	+0.74[b]	−0.97	−1.08	−1.30	−1.62[b]
[qRu(1pRu)$_6$]$^{2+}$		+1.24[b]	+0.75[b]	−0.94	−1.05	−1.32	−1.66[b]
[qRu(2pRu)$_6$]$^{2+}$		+1.12[b]	+0.59[b]	−0.97[a]	−1.10	−1.30	

[a] Complicated by a subsequent chemical reaction, peak potential values from differential pulse voltammetry. [b] Six-electron process.

while the second one is more negative in the cases of the Ru and Os complexes than that for the Fe complex. This suggests there is a minor electronic communication between the pytpy units in the last complex. In all cases the reduction processes are only partially reversible.

Judging by Figures 5b−d, it is evident that the oxidation and reduction processes of the supramolecular species **[tM(1pRu)$_2$]**$^{2+}$ can be described as the superposition of the oxidation and reduction processes of the respective components, **1pRu** and **tM**$^{2+}$. In reality, **[tRu(1pRu)$_2$]**$^{2+}$ and **[tOs(1pRu)$_2$]**$^{2+}$ display three anodic processes, with current intensity ratio 2:2:1 and 2:1:2, respectively. The bielectronic nature of the first oxidation has been confirmed by controlled potential coulometry ($E_w = +0.9$ V), which also proved the chemical stability of the electrogenerated tetracation. By comparison with **1pRu**, the two bielectronic processes are attributed to the simultaneous oxidation of the two Ru-porphyrin fragments, which are therefore essentially noninteracting, whereas the interposed or following monoelectronic processes are assigned to the oxidation of the central metal ions. In turn, compound **[tFe(1pRu)$_2$]**$^{2+}$ exhibits two anodic processes, with a current ratio of 2:3. Also in this case, the bielectronic nature of the first oxidation has been confirmed by controlled potential coulometry ($E_w = +0.9$ V), which also revealed the slow decompostion of the tetracation. Comparison of the redox potentials of **1pRu** and **tFe**$^{2+}$ suggests that the oxidation of the iron ion overlaps the second oxidation of the porphyrin units. All the three compounds, **[tM(1pRu)$_2$]**$^{2+}$, show three reductions with current ratios of 1:1:2. By comparison with **tM**$^{2+}$, it is straightforward to assign the first two cathodic processes as centered on the pytpy ligands. The small decrease of electron density caused by the coordination of the pytpy ligands to Ru(ttp)CO units is proved by the slight anodic shift (50−100 mV) with respects to **tM**$^{2+}$. Finally, the third reduction is attributed to the porphyrin-centered bielectronic process. It is noted that an analogous redox pattern has been observed in the series of mixed metallic wires $[Ru(tpy)_2-(C\equiv C)_n-M(tpy)_2(C\equiv C)_nRu(tpy)_2]^{6+}$ (n = 1,2; M = Zn^{II}, Fe^{II}, or Co^{II}), which have a topology

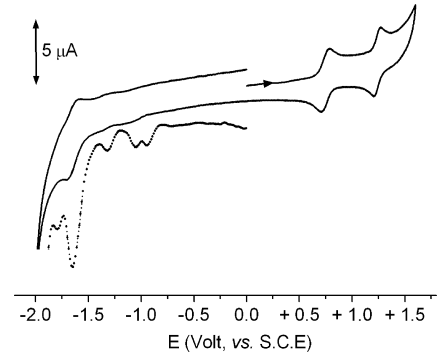

Figure 6. Cyclic (full line) and differential pulse (dotted line) voltammetric responses recorded at the platinum electrode in CH_2Cl_2 solutions containing **[qRu(1pRu)$_6$]**$^{2+}$ (0.2×10^{-3} mol dm^{-3}). $[NBu_4][PF_6]$ (0.2 mol dm^{-3}) supporting electrolyte. Scan rate, 0.2 V s^{-1}.

similar to compounds **[tM(1pRu)$_2$]**$^{2+}$.[31] In fact, also in these cases, the redox potentials for the oxidation of the peripheral ruthenium centers are almost unaffected by the nature of the metal in the bridging units.

Considering the complexes illustrated in Chart 2, it is preliminarily stated that the redox behavior of the building unit $[Ru(quad)_3]^{2+}$ (**qRu**$^{2+}$) is rather similar to that observed for $[Ru(pytpy)_2]^{2+}$ (**tRu**$^{2+}$). An ill-defined oxidation is conceivably ascribed to the redox change Ru(II)/Ru(III) which is coupled to adsorption effects, whereas the appearance of three chemically reversible one-electron reductions is assigned to the sequential reduction of the three quad units. The pertinent electrode potentials are compiled in Table 4.

The heptametallic species **[qFe(1pRu)$_6$]**$^{2+}$, **[qRu(1pRu)$_6$]**$^{2+}$, and **[qRu(2pRu)$_6$]**$^{2+}$ display rich redox patterns. The cyclic voltammogram of **[qRu(1pRu)$_6$]**$^{2+}$ illustrated in Figure 6 exemplifies their behavior.

As far as the anodic path is concerned, two six-electron processes are detected, the redox potentials of which match with those of the first two oxidations of **1pRu** or **2pRu** moieties in **[qM(1pRu)$_6$]**$^{2+}$ and **[qRu(2pRu)$_6$]**$^{2+}$, respectively. These processes therefore are due to the concomitant oxidations of the six independent Ru-porphyrin units.

(31) (a) Grosshenny, V.; Harriman, A.; Ziessel, R. *Angew. Chem.* **1995**, *107*, 2921. (b) Grosshenny, V.; Harriman, A.; Ziessel, R. *Angew. Chem., Int. Ed. Engl.* **1995**, *34*, 2705.

Table 5. Formal Electrode Potentials (V vs SCE) for the Redox Processes Exhibited By CH_2Cl_2 Solutions of the Complexes Shown in Chart 3

compound	oxidation processes			reduction processes[a]	
1bCu$^+$		+1.17[a]	+0.77		−1.66
[2bCu(1pRu)$_4$]$^+$	+1.26[b]		+0.74[c]	−1.27	−1.55

[a] Complicated by a subsequent chemical reaction. [b] Four-electron process. [c] Five-electron process.

In the cathodic region, four reductions are seen for **[qM(1pRu)$_6$]**$^{2+}$. While it has not been possible to establish reliably the number of exchanged electrons, the differential pulse voltammetry clearly indicates that the first three reduction processes have similar intensities, while the more cathodic peak observed is more intense. Comparison with **qRu**$^{2+}$ and **1pRu** allows the assignment of the first three processes to the sequential one-electron reduction of the three quad units, while the most cathodic process is ascribed to the simultaneous reduction of the six independent porphyrin rings. On the other hand, as expected, for **[qRu(2pRu)$_6$]**$^{2+}$ only the three reductions of the quad units are detected. In these complexes the electron density lost by the "quad" ligands coordinated to *two* Ru(ttp)CO units is more important than in **[tM(1pRu)$_2$]**$^{2+}$, where each pytpy ligand coordinates just *one* Ru(ttp)CO unit. This is further confirmed by a more important anodic shift (150−220 mV) of the "quad" reductions in **[qM(1pRu)$_6$]**$^{2+}$ with respect to **qRu**$^{2+}$. Thus, the M(II) ion in the central M(quad)$_3$ unit is likely also deprived of electron density so that its oxidation is anodically shifted beyond the solvent discharge. It is noted that the first oxidation of the peripheral Ru(ttp)CO units occurs at the same potential value both in the neutral Ru-porphyrin systems and in the charged heptanuclear supermolecule, as it happens for the second oxidation of the monocationic [**1pRu**]$^+$ or [**2pRu**]$^+$ and that of the highly charged **[qM(1pRu)$_6$]**$^{8+}$ or **[qM(2pRu)$_6$]**$^{8+}$. In fact, it has been previously observed that in weakly coupled supramolecular assemblies, the electrochemical properties of the building blocks depend only on the neighbors, regardless of the nuclearity and of the overall charge of the compound.[4]

Finally, let us discuss the redox behavior of complexes shown in Chart 3. Copper usually produces tetra-coordinate bis(bipyridine) complexes whose geometry is interchanged between tetrahedral Cu(I) and square planar Cu(II) by a reversible redox reaction.[32] The CV of **1bCu**$^+$ shows a reversible oxidation at potential value considerably more positive than that of unsubstituted $[Cu(bpy)_2]BF_4$ ($E°' \cong +0.20$ V)[32] (Table 5).

As suggested by Nishihara et al.,[32] such a positive shift can be attributed to the effect of steric hindrance of the phenyl groups in the 6,6′-positions of ph$_4$bpy, which prevents the formation of the more favorable square planar structure in the Cu(II) state. The subsequent Cu(II)/Cu(III) oxidation process is chemically irreversible because in the present complex Cu(III) cannot achieve the preferred square planar geometry. Complex **1bCu**$^+$ also undergoes a chemically irreversible reduction process, the current intensity of which is apparently at least twice that of the oxidation. The attribution of this cathodic process is not straightforward; in fact, a similar behavior is displayed by the rather similar complex, $[Cu(me_2ph_2bpy)]BF_4$ (me$_2$ph$_2$bpy = bis(4,4′-dimethyl-6,6′-diphenyl-2,2′-bipyridine)) and has been described as a possible electrocatalytic process but not studied in detail.[33] A reduction process has been also detected for a Cu(bpy)-containing conductive polymer and assigned as a Cu(I)/(0) couple.[34] As a matter of fact, the ph$_4$bpy ligand is also redox active; therefore, an unambiguous attribution of the cathodic process is not easy.

The pentametallic species **[2bCu(1pRu)$_4$]**$^+$ only shows two oxidation processes, the redox potentials of which also match with those of the first two oxidations in **1pRu**. Nevertheless, as confirmed by the EPR measurements discussed below, in this case, the first oxidation overlaps with the Cu(I)/Cu(II) redox change of the central copper ion. In fact, the current intensity ratio, as measured by a differential pulse voltammetry, is 5:4. This result indicates that the oxidation of the peripheral porphyrin units and of the central Cu(I) ion proceed at the same potential, as further supported by the EPR experiments. In the cathodic region two signals appear. Tentatively, the first, partially reversible, process can be attributed to the ph$_2$quad centered reduction. In fact, upon coordination to two Ru(ttp)CO units, the electronic density of the ph$_2$quad ligands is reduced, so making their reduction easier than in **1bCu**$^+$ where such a process was not detected in the experimental window. Less straightforward is the assignment of the second irreversible process. In fact, the reduction of **1pRu** in all the previously examined polynuclear complexes were almost unaffected. It cannot be ruled out that such a process could belong to the fragment **2bCu**$^+$.

In conclusion, it is worth underlining that, in this family of compounds, species with predetermined redox patterns can be obtained via the synthetic control of the supramolecular structure. The possibility to exchange a well defined number of electrons at a certain potential is interesting for the design of molecular batteries and in the field of multielectron-transfer catalysis.[35] Additionally, it should be noted that the electrochemical data offer a fingerprint of the chemical and topological structure of such supermolecules.

EPR Measurements. The cations **1pRu**$^+$ **[tM(1pRu)$_2$]**$^{3+}$ (M = Fe, Ru, Os) and **[2bCu(1pRu)$_4$]**$^{2+}$, electrogenerated by removing a single electron via electrolysis (E_w = +1.0 V) of a solution of CH_2Cl_2 at −20 °C under an inert atmosphere, have been characterized by X-band EPR spectroscopy at different temperatures (T = 103 and 298 K, respectively). Figures 7 and 8 show the EPR spectra of the S = 1/2 cations **1pRu**$^+$ and **[tM(1pRu)$_2$]**$^{3+}$ (M = Fe, Ru,

(32) (a) Kume, S.; Murata, M.; Ozeki, T.; Nishihara, H. *J. Am. Chem. Soc.* **2005**, *127*, 490. (b) Nishihara, H. *Coord. Chem. Rev.* **2005**, *249*, 1468. (c) Kume, S.; Kurihara, M.; Nishihara, H. *Inorg. Chem.* **2003**, *42*, 2194.

(33) Williams, R. M.; De Cola, L.; Hartl, F.; Lagref, J.-J.; Planeix, J.-M.; De Cian, A.; Hosseini, W. *Coord. Chem. Rev.* **2002**, *230*, 253.

(34) Maruyama, T.; Yamamoto, T. *Inorg. Chim. Acta* **1995**, *238*, 9.

(35) Astruc, D. *Pure Appl. Chem.* **2003**, *75*, 461.

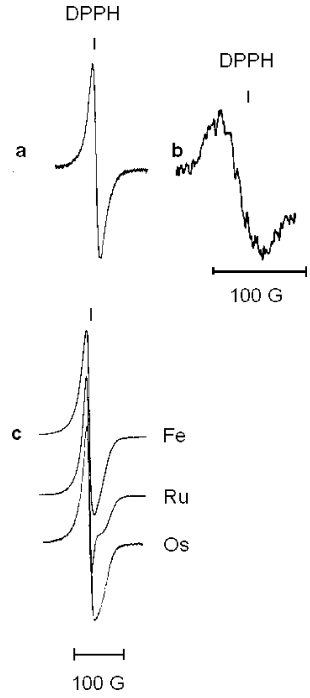

Figure 7. X-Band EPR spectra recorded on a CH_2Cl_2 solution containing $[NBu_4][PF_6]$ (0.2 mol dm^{-3}) and the electrogenerated cations **1pRu**$^+$: (a) frozen solution (T = 115 K)), (b) fluid solution (T = 190 K), (c) **[tM(1pRu)$_2$]$^{3+}$** (M = Fe (top), Ru (middle), Os (bottom), frozen solution (T = 115 K).

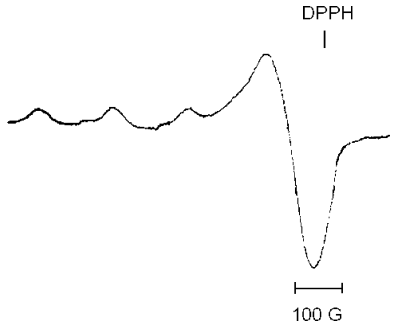

Figure 8. X-Band EPR spectrum recorded on a CH_2Cl_2 solution containing $[NBu_4][PF_6]$ (0.2 mol dm^{-3}) and the electrogenerated cations **[2bCu(1pRu)$_4$]$^{2+}$**, frozen solution (T = 115 K).

Os) and **[2bCu(1pRu)$_4$]$^{2+}$**, respectively. Table 6 compiles the relevant EPR parameters as derived from computer simulation of the experimental spectra at different temperatures assuming a $S = 1/2$ Spin Hamiltonian (M^{2+} in LS state).[36]

The EPR features of **1pRu**$^+$ and **[tM(1pRu)$_2$]$^{3+}$** glassy solutions are quite identical. The lineshapes are significantly narrow and the related $g_{\mathbf{aniso}}$ values ($\langle g \rangle = 2.002-2.003$) are consistent with ligand centered paramagnetic complexes, as in the case of the well-known carbonyl ruthenium(II) porphyrins π-cation complexes which typically display a single sharp signal with $g = 2.000$[29] (at room temperature). As a matter of fact, the glassy EPR spectra of both **1pRu**$^+$ and **[tM(1pRu)$_2$]$^{3+}$** show the presence of two paramagnetic species (sum spectra). The line shape analysis indicates that the lower field signals are more intense than those positioned at higher field and partially overlapped to the minor ones. Interestingly, in fluid solution condition (265 K) a single signal is detected in all cases, with g_{iso} values in the 2.000−2.002 range. Accordingly, rapidly refreezing the fluid solutions only a single narrow absortion is recovered, corresponding to the previous low-field one and exhibiting reduced spectral anisotropy. This allow us to identify the high-field minor species as a transient paramagnetic byproduct. The main signals of the **1pRu**$^+$ and **[tM(1pRu)$_2$]$^{3+}$** species are suitably simulated as slightly axial. The small differences between the corresponding values of $g_{\parallel}$ and $g_{\perp}(\delta g_i = |g_{\perp} - g_{\parallel}|_i = 0.008-0.015$; $g_{iso} \approx \langle g \rangle$) suggest the absence of significant structural distortions.[37] It is noted that the fluid solution EPR spectrum of **1pRu**$^+$ (first derivative mode) exhibits some resolved splittings, at least seven lines (a_{hpf} = 10 G), consistent with the hyperfine coupling of the unpaired electron with the nitrogen nuclei (^{14}N; I = 1; natural abundance = 99.6%) of the porphyrin ring; on the other side, there is no EPR evidence for magnetic interaction of the unpaired electron with the two ^{99}Ru (I = 5/2; natural abundance = 10.2%) and ^{101}Ru (I = 5/2, natural abundance = 14.8%) isotopes. On the contrary, the fluid solution spectra (T = 298K) of the **[tM(1pRu)$_2$]$^{3+}$** series are unresolved both in first and second derivative mode. Accounting for the experimental linewidths, upper limits for the related hyperfine couplings could be computed ($\Delta H_{iso} \geq a_{iso}(^{14}N)$). Because the isotropic linewidths of the **1pRu**$^+$ and **[tM(1pRu)$_2$]$^{3+}$** are quite identical, it is interesting to note that the ^{14}N best fit hyperfine coupling of complex **1pRu**$^+$ is about double in magnitude with respect to those of the **[tM(1pRu)$_2$]$^{3+}$** compounds. This trend indicates a major magnetic interaction of the unpaired electron with the four porphyrinic nitrogen atoms and could be a sign of the different ground-state of the π cations in **1pRu**$^+$ and **[tM(1pRu)$_2$]$^{3+}$.** In fact, it is known that the unpaired spin density in the $^2A_{2u}$ ground-state resides mainly on the nitrogens and meso carbon atoms, while the $^2A_{1u}$ ground-state has most of the unpaired spin density on the α-pyrollic carbons.[38]

As expected on the basis of the electrochemical results, the EPR features of **[2bCu(1pRu)$_4$]$^{2+}$** are totally different from those observed for **1pRu**$^+$ and **[tM(1pRu)$_2$]$^{3+}$** in that they are dominated by the fundamental Cu(II) spin−orbit contribution to g_i and a_i(Cu). Figure 8 shows the frozen solution EPR spectrum, typically metal-in-character.

The spectrum exhibits a broad axial pattern, with three of the expected four hyperfine transitions well visible in the parallel region (low-field range), whereas the fourth component is masked by the overlap with the relevant $g_{\perp}$ features in the high-field region, which is unresolved. The

(36) (a) Romanelli, M. (S = 1/2) "Anisotropic EPR simulation package", home-made program, Università di Firenze, 1995;(b) Della Lunga, G.;"ESRMGR simulation program", home-made program, Università di Siena, 1998.

(37) Mabbs, F. E.; Collison, D.; *Electron Paramagnetic Resonance of d Transition Metal Compounds.*; Elsevier: London, 1992; Vol. *16*, Studies in Inorganic Chemistry.

(38) Skillman, A. G.; Collins, J. R.; Loew, G. H. *J. Am. Chem. Soc.* **1992**, *114*, 9538.

Table 6. Temperature Dependent X-Band EPR Parameters of the Complexes under Study

compound	$g_{\|\|}$	$g_\perp$	$\langle g \rangle$	g_{iso}	$a^a_{\|\|}$	$a^a_\perp$	$\langle a^a \rangle$	a^a_{iso}
1pRu$^+$	1.996(10)[b]	2.005(3)	2.002(6)	2.002(5)	≤6(4)[c]	≤6(2)	≤6(2)	10(4)
[tFe(1pRu)$_2$]$^{3+}$	1.992(10)[b]	2.007(3)	2.002(6)	2.002(5)	≤3(4)[c]	≤3(2)	≤3(2)	≤5(2)
[tRu(1pRu)$_2$]$^{3+}$	1.998(10)[b]	2.006(3)	2.003(6)	2.000(5)	≤1(4)[c]	≤1(2)	≤1(2)	≤4(2)
[tOs(1pRu)$_2$]$^{3+}$	1.997(9)[b]	2.005(2)	2.002(5)	2.002(5)	≤2(4)[c]	≤2(2)	≤2(2)	≤6(2)
[2bCu(1pRu)$_4$]$^{2+}$	2.254(5)	2.036(5)	2.109(5)	2.133(5)	162(8)	≤27(8)	≤72(8)	75(8)

[a] In Gauss. [b] Calculated by g_{iso} and $g_\perp$. [c] Calculated by a_{iso} and $a_\perp$; $\langle g \rangle = 1/3(g_{||} + 2g_\perp)$, $\langle a \rangle = 1/3(a_{||} + 2a_\perp)$.

Table 7. Photophysical Properties in Deaerated CH_2Cl_2 Solution, Unless Otherwise Noted

	absorption		luminescence				
	λ_{max}/nm ($\varepsilon \times 10^{-3}$/M^{-1} cm^{-1})		298 K			77 K[a]	
compound	MLCT	Q bands	λ/nm[b]	τ/μs	Φ_{em}	λ/nm[b]	τ/μs
1pRu		533 (19.1) 568 (5.5)	738	26	0.0016	733	210
2pRu		517 (16.1) 549 (25.0)	659	33	0.0037	653	600
[tFe(1pRu)$_2$]$^{2+}$	*c*	528 (38.1) 565 (29.2)[c]					
[tRu(1pRu)$_2$]$^{2+}$	489 (48.2)[d]	529 (54.2)[d] 561sh (10.0)	728	31	0.0022	725	250
[tOs(1pRu)$_2$]$^{2+}$	492 (37.9)[d] 674 (6.48)	532 (43.0)[d] 567 (14.8)	758	0.013	0.0006	728	11, 71[e]
[qRu(1pRu)$_6$]$^{2+}$		532 (106.0) 567 (31.7)	731	46	0.0009	724	200
[qRu(2pRu)$_6$]$^{2+}$		516 (86.9) 548 (115.0)	660	6.1, 40[f]	0.0001	651	770
tFe^{2+}	565 (18.2)						
tRu^{2+}	486 (17.7)		≈640	0.250 ns	$<3 \times 10^{-5}$	598	11
tOs^{2+}	482 (13.7) 663 (3.6)		718	0.269	0.014	689	3.9
[Os(bpy)$_3$](PF$_6$)$_2$[g]	480 (8.7) 579 (1.9)		742	0.060	0.005	709	0.79

[a] In CH_2Cl_2/$CHCl_3$ 1:1 v/v. [b] Uncorrected for detector response. [c] MLCT of the core Fe-pytpy units overlaps the low energy Q-band. [d] ε is difficult to evaluate because of partial overlap. [e] Multiexponential decay: 11 (83%), 71 (17%); [f] 6.1 multiexponential decay: (98%), 40 (2%). SPC suggests also a shorter decay, ≈3 μs. [g] In acetonitrile (298 K) and in MeOH/EtOH 4:1 v/v (77 K).

computed anisotropic g_i values ($g_{||} = 2.254$, $g_\perp = 2.036$, $\langle g \rangle = 2.109$; $g_i \rangle g_{electron} = 2.0023$) and the related hyperfine $a_{||}$ value (162 G) are in the middle of the range of values spanned by changing the coordination geometry from tetrahedral to square planar arrangement,[39] suggesting an highly distorted tetrahedral geometry. Such a distortion significantly reflects the broad axial line width with limited hyperfine(Cu) and superhyperfine(N) resolution.[37] The g_{iso} and a_{iso} parameters of the fluid solution spectrum as well as the corresponding $\langle g \rangle$ and $\langle a \rangle$ of the solid state one, recorded on the electrolyzed solution after evaporation, are in good accordance, indicating that the coordinating skeleton of the complex is basically maintained under different experimental conditions.

Spectroelectrochemistry and Photophysical Properties. The UV−vis spectrum of **1pRu** is typical for a Ru(por-)(CO)(py) compound,[40] and it shows an intense Soret band at 405 nm and two Q-bands at 533 and 568 nm. The visible spectra of complexes **tM**$^{2+}$ show only a MLCT band,[41] with the exception of **tOs**$^{2+}$, which also shows the forbidden ^{3}MLCT band.[30] The absorption in the UV region are assigned to pytpy-based $\pi-\pi^*$ bands.[41] As previously reported,[7] the UV−vis spectra of **[tM(1pRu)$_2$]**$^{2+}$ are basically the sum of the absorption spectra of the constituents. Absorption data relative to the Q-bands of these compounds are collected in Table 7, together with data concerning mononuclear Os and Ru complexes useful for comparison purposes.

The *in situ* spectroelectrochemistry of compounds **1pRu** and **[tM(1pRu)$_2$]**$^{2+}$ has been studied by collecting spectra during a cyclic potential scan at 0.5 mV/s in the +0.3 to +1.0 V potential range in an OTTLE cell, that is in correspondence of the first oxidation step. The formation of **1pRu**$^+$ causes the blue-shift of about 100 nm of the Soret band and the disappearance of the original Q-bands. At the same time three new broad bands appear at 583, 636, and 738 nm, Figure 9a.

This spectrum is characteristic of the π-cation radicals of porphyrin rings, as observed in the Zn^{II}, Co^{III}, and Ru^{II}(CO) porphyrin complexes.[42] The presence of five isosbestic points confirms the stability of the electrogenerated cation. A similar behavior is also exhibited by the triads **[tM(1pRu)$_2$]**$^{2+}$. In fact, the removal of the first two electrons generates a final spectrum perfectly matching that for **1pRu**$^+$, with the addition of the unperturbed MLCT band(s) due to the central M(ptpy)$_2$ unit. The difference in the Soret band bandwidth is ascribed to the different concentration used in the

(39) Baumann, F.; Livoreil, A.; Kaim, W.; Sauvage, J.-P. *J. Chem. Soc., Chem. Commun.* **1997**, 35.
(40) Bonnet, J. J.; Eaton, S. S.; Holm, R. H.; Ibers, J. A. *J. Am. Chem. Soc.* **1973**, *95*, 2141.
(41) Maestri, M.; Armaroli, N.; Balzani, V.; Constable, E. C.; Cargill Thompson, A. M.W. *Inorg. Chem.* **1995**, *34*, 2759.
(42) (a) Brown, G. M.; Hopf, F. R.; Ferguson, J. A.; Meyer, T. J.; Whitten, D. G. *J. Am. Chem. Soc.* **1973**, *95*, 5939. (b) Wolberg, A.; Manassen, J. *J. Am. Chem. Soc.* **1970**, *92*, 2982.

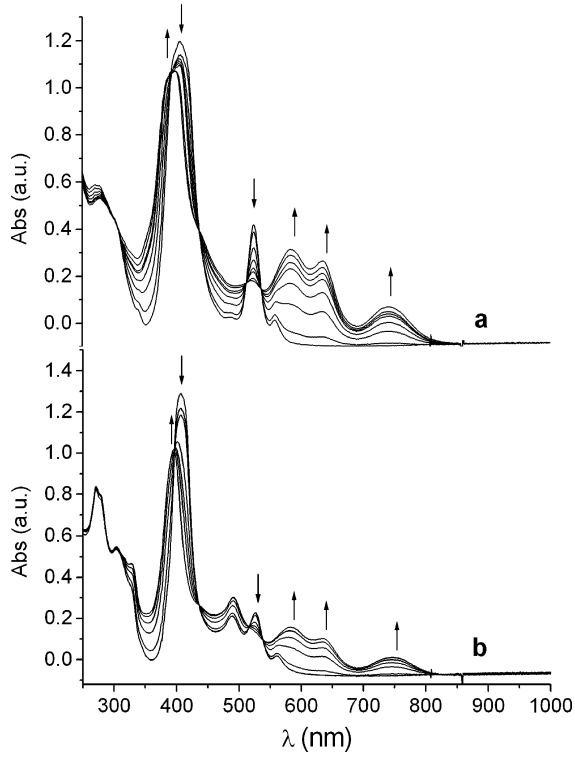

Figure 9. OTTLE cell UV−vis−NIR spectra showing changes on oxidation of (a) **1pRu**, (b) $[\mathbf{tRu(1pRu)_2}]^{2+}$ in CH_2Cl_2 containing $[NBu_4][PF_6]$ (0.2 mol dm^{-3}) as the supporting electrolyte. Spectra were collected during a cyclic potential scan at 0.5 mV/s in the +0.3 to +1.0 V potential range.

experiments. In fact, a broadening of the Soret band, or even the presence of two split bands, has been reported for aggregated systems of porphyrins.[43] In Figure 9b, the spectroelectrochemical changes of $[\mathbf{tRu(1pRu)_2}]^{2+}$ upon oxidation at the first step are shown as an example.

As far as luminescence is concerned, emission was not observed from the Fe- and Cu-containing compounds. On the contrary, all of the other species were luminescent both at room temperature and at 77 K. The reference compounds **1pRu** and **2pRu** show a phosphorescence emission, the first one being strongly red-shifted with respect to the latter, both at room temperature and at 77 K. The data (Table 7) are in good agreement with those reported in the literature for similar compounds.[2,44]

Figure 10 shows the absorption and emission spectra of compounds $[\mathbf{tRu(1pRu)_2}]^{2+}$, $[\mathbf{tOs(1pRu)_2}]^{2+}$, and $[\mathbf{qRu(2pRu)_6}]^{2+}$, while Figure 11 outlines an energy-level diagram of the various states that can be reached after light excitation in these three species. As usual, the energy of the excited states is determined by using luminescence data, whereas the energy of redox-separated states is estimated from

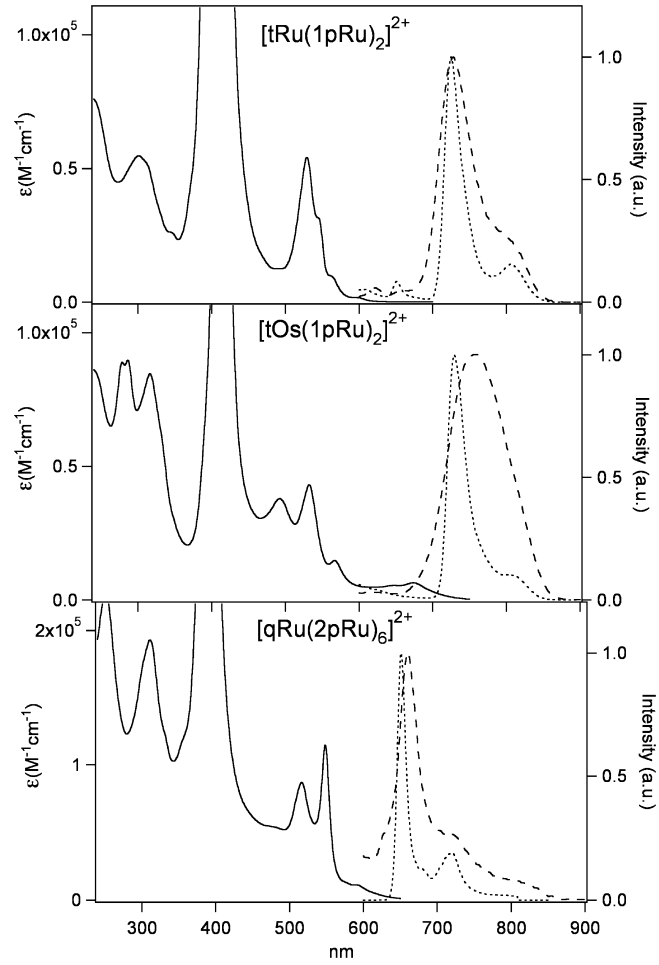

Figure 10. Absorption spectra of compounds $[\mathbf{tRu(1pRu)_2}]^{2+}$, $[\mathbf{tOs(1pRu)_2}]^{2+}$, and $[\mathbf{qRu(2pRu)_6}]^{2+}$ (solid line) and their uncorrected luminescence spectrum at room temperature in CH_2Cl_2 solution (dashed line), and at 77 K in $CH_2Cl_2/CHCl_3$ 1:1 v/v matrix (dotted line).

electrochemical data.[45] As far as the redox-separated states are concerned, the work term corrections have been neglected because in similar cases such corrections have been shown to be small. [45]

Compound $[\mathbf{tRu(1pRu)_2}]^{2+}$ again shows the typical luminescence spectrum of its reference compound **1pRu**, with similar excited-state lifetime and luminescence quantum yields. These findings are in agreement with the electrochemical data, which indicate that the possible charge transfer states lie at higher energy with respect to the luminescent state, as illustrated in Figure 11. As unambiguously supported by the fact that the excitation spectrum closely resembles the absorption one, in $[\mathbf{tRu(1pRu)_2}]^{2+}$ all the absorbed energy is ultimately transferred to a peripheral Ru(ttp)CO moiety, where emission takes place.

A very similar behavior is observed for $[\mathbf{qRu(1pRu)_6}]^{2+}$, in which again the energy appears efficiently funneled to a peripheral Ru porphyrin moiety, as supported by the excitation spectra.

A completely different behavior was observed for $[\mathbf{tOs(1pRu)_2}]^{2+}$, which, at room temperature, shows a lower-energy luminescence having features very similar to that

(43) (a) Iengo, E.; Zangrando, E.; Bellini, M.; Alessio, E.; Prodi, A.; Chiorboli, C.; Scandola, F. *Inorg. Chem.* **2005**, *44*, 9752. (b) Khairutdinov, R. F.; Serpone, N. *J. Phys. Chem. B.* **1999**, *103*, 761. (c) Stibrany, R. T.; Vasudevan, J.; Knapp, S.; Potenza, J. A.; Emge, T.; Schugar, H. J. *J. Am. Chem. Soc.* **1996**, *118*, 3980.

(44) (a) Levine, L. M. A.; Holten, D. *J. Phys. Chem.* **1988**, *92*, 714. (b) Stulz, E.; Sanders, J. K. M.; Montalti, M.; Prodi, L.; Zaccheroni, N.; Fabrizi de Biani, F.; Grigiotti, E.; Zanello, P. *Inorg. Chem.* **2002**, *41*, 5269. (c) Mak, C. C.; Bampos, N.; Darling, S. L.; Montalti, M.; Prodi, L.; Sanders, J. K. M. *J. Org. Chem.* **2001**, *66*, 4476–4486.

(45) Jones, W. E.; Bignozzi, C. A.; Chen, P.; Meyer, T. J. *Inorg. Chem.* **1993**, *32*, 1167.

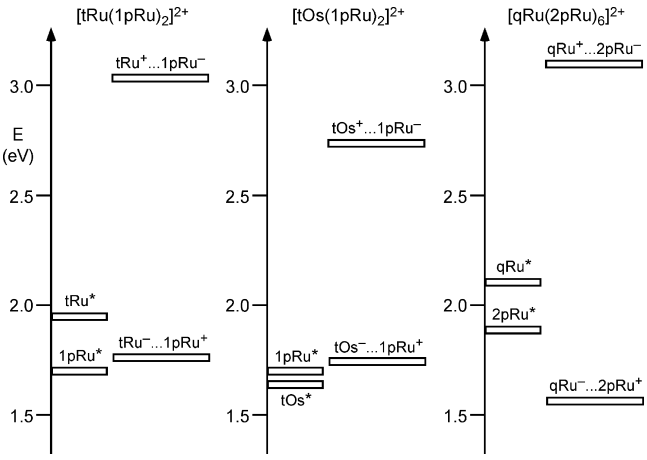

Figure 11. Energy-level scheme for the compounds $[tRu(1pRu)_2]^{2+}$, $[tOs(1pRu)_2]^{2+}$, and $[qRu(2pRu)_6]^{2+}$, valid at room temperature. For each species, the spectroscopic states (left column) are indicated separately from the redox-separated states (right column). For brevity, each level is labeled with the involved fragment only; for example, $tRu^{-}\cdots 1pRu^{+}$ indicates a charge-separated state where an electron has been transferred from the 1pRu unit to a tRu unit.

observed for Os polypyridine complexes (less structured band, lifetime in the nanosecond range). As for $[tRu(1pRu)_6]^{2+}$ and $[qRu(1pRu)_6]^{2+}$, the excitation spectra closely resemble the absorption ones, clearly indicating that in these conditions an energy transfer process from the peripheral Ru porphyrin to the central Os complex occurs, that is, in the opposite direction with respect to that observed for the compounds with Ru(II) in the core unit. As indicated in Figure 11, the possible charge-separated states lie at higher energy with respect to the luminescent state. The behavior of $[tOs(1pRu)_2]^{2+}$ at 77 K is more complicated because in these experimental conditions the presence of two distinct excited-state lifetimes can be observed. It is important to underline that, while the energy of the excited-state centered on the Ru porphyrin is expected to be almost unaffected by the lowering of the temperature to 77 K and the subsequent freezing of the matrix, the luminescent MLCT state centered on the Os complex is expected to be destabilized, thus leading to an increase of its energy. This leads to a situation in which the two triplet states lie very close one another so that, if a thermal equilibrium is not reached, two lifetimes can be observed.

An even different situation is observed for $[qRu(2pRu)_6]^{2+}$. In this case, the shape of the luminescence spectrum is very similar to that one of the **2pRu** parent complex, but at room temperature the lifetime and luminescence quantum yield are in contrast substantially reduced. In this supermolecule, electron transfer quenching of the luminescent state centered on a peripheral porphyrin unit is possible because of the presence of a lower energy charge-separated state in which an electron is transferred from one of the porphyrins to the core polypyridine complex (Figure 11). Transient absorption spectra recorded following laser flash excitation of $[qRu(2pRu)_6]^{2+}$ at room temperature failed, however, to provide evidence for the presence of the core reduced ruthenium species or an oxidized porphyrin unit. This can be justified by considering that the difference spectrum Ru(II)/Ru(I) is expected to feature a band around 510 nm (covered by the porphyrins absorption) and that only one of the six porphyrins is oxidized in the charge-separated state. Support for the electron transfer quenching hypothesis comes, on the other hand, from the lack of quenching processes observed at 77 K, where charge separated states are strongly destabilized.

Conclusions

In the design of supramolecular assemblies, great care has to be taken in the choice of the building blocks to obtain a predefinite energy or electron transfer funnelling process. The design of large porphyrin assemblies is an important field of research, mainly because of the attractive photophysical and electrochemical properties of the porphyrin unit. On the other hand, the favorable photophysical properties of polypyridine Ru(II) and Os(II) complexes make them useful photosensitizers in multicomponent systems. Once bpy or tpy are functionalized with electron donor groups, very versatile linkers are obtained for use in the design of multicomponent systems. In particular, the formation of coordination bonds between the peripheral donor sites of "pytpy" and "quad" ligands and the ruthenium centers of Ru(CO)-porphyrins has been found to be a very convenient approach for the construction of discrete, ordered supramolecular assemblies. Moreover, with the "quad" ligand, very high nuclearity supermolecules can be obtained. The photophysical and redox behavior of this series of polynuclear species containing Ru(ttp)CO or Ru(oep)CO units axially linked to a central Fe(II), Ru(II), Os(II), or Cu(I) core by polypyridine bridging ligands has been charaterized. The redox features of the building blocks are scarcely affected by the formation of the supramolecular assembly, suggesting that there is no significant electronic coupling between them. On the other side, new photophysical properties appear. In particular, the change of the central metal $[tM(1pRu)_2]^{2+}$ from ruthenium to osmium in the linear arrays reverses the direction of the energy transfer. The efficient sensitization of $Os(tpy)_2$-like complexes is a very interesting result because these complexes typically present a fairly intense luminescence, relatively unaffected by the presence of molecular oxygen, in a spectral region that is very attractive for the design of labels and sensors for medical diagnostics and biological applications.[46] The photophysical properties of the compounds described in this paper are of considerable interest because of the occurrence of intercomponent energy transfer processes whose direction can be controlled by the metal present in the linker. It is reasonable to envisage that the direction and/or efficiency of the energy transfer could be also systematically controlled by changes in the characteristics of the frontier molecular orbitals of the porphyrin. This can be obtained in many different ways, for example, by changing the central metal or with an apical ligand different from carbonyl. In perspective, this possibility opens the way to a very fine control of the energy flow.

(46) Prodi, L. *New J. Chem.* **2005**, *29*, 20.

Acknowledgment. Dr. R. McDonald is gratefully acknowledged for the X-ray diffraction and reflectivity measurements. A.J. and L.P. gratefully acknowledge the financial support of MIUR through FIRB 2003−2004 LATEMAR (http://www.latemar.polito.it), P.Z. and F. F. de B. gratefully acknowledge the financial support of the University of Siena (PAR Progetti 2005 and PAR 2006). N.R.B. and K.C. gratefully acknowledge the financial support of the Natural Sciences and Engineering Research Council of Canada and the University of Alberta.

Supporting Information Available: Listings of the synthesis procedure, NMR, and selected IR (microscope) and MS (ESI+) characterizations of the compounds. This material is available free of charge via the Internet at http://pubs.acs.org.

IC7018428